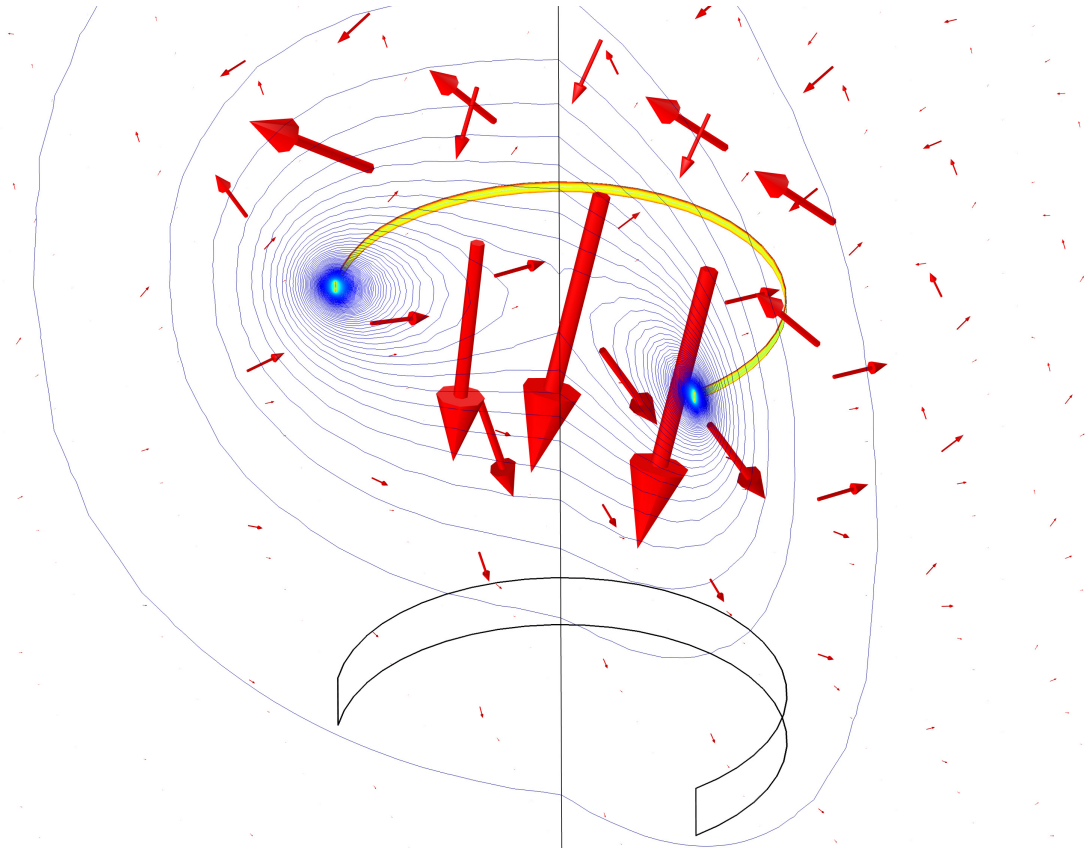




**CHALMERS**  
UNIVERSITY OF TECHNOLOGY

---



# Wireless power transfer using resonant inductive coupling

Design and implementation of an IPT system with one meter  
air gap in the region between near-range and mid-range

Master's thesis in Electric Power Engineering

MARIA NISSHAGEN  
EMMA SJÖSTRAND



MASTER'S THESIS 2017:06

# Wireless power transfer using resonant inductive coupling

Design and implementation of an IPT system with one meter air gap  
in the region between near-range and mid-range

MARIA NISSHAGEN  
EMMA SJÖSTRAND



Department of Energy and Environment  
*Division of Electric Power Engineering*  
CHALMERS UNIVERSITY OF TECHNOLOGY  
Gothenburg, Sweden 2017

Wireless power transfer using resonant inductive coupling  
Design and implementation of an IPT system with one meter air gap in the region  
between near-range and mid-range  
MARIA NISSHAGEN  
EMMA SJÖSTRAND

© MARIA NISSHAGEN  
EMMA SJÖSTRAND, 2017.

Supervisor: Richard Kahl, Sigma Embedded Engineering  
Examiner: Yujing Liu, Energy and Environment

Master's Thesis 2017:06  
Department Energy and Environment  
Division of Electric Power Engineering  
Chalmers University of Technology  
SE-412 96 Gothenburg  
Telephone +46 31 772 1000

Cover: Magnetic flux density visualization simulated in COMSOL Multiphysics®

Typeset in L<sup>A</sup>T<sub>E</sub>X  
Printed by Chalmers Reproservice  
Gothenburg, Sweden 2017



Wireless power transfer using resonant inductive coupling

MARIA NISSHAGEN

EMMA SJÖSTRAND

Department of Energy and Environment

Division of Electric Power Engineering

Chalmers University of Technology

## Abstract

Wireless power transfer (WPT) is the transmission of energy from a source to an electrical load over an air gap without using physical contact. One of the most common magnetic coupling WPT is the resonant inductive power transfer (IPT). It is a system which consist of at least one sending and one receiving coil which resonates to make the circuit appear resistive, thus decreasing the reactive power in the system and increasing the active power transfer. The IPT system can be classified to be either near-range or mid-range. Mid-range is when the distance between the coils is larger than the coil dimensions and near-range is when the distance between the coils is smaller than the coil dimension.

The development of IPT technology has increased rapidly during the last couple of years, due to increased use of electrical vehicles and portable devices such as phones and laptops. Since resonant IPT is necessary to use where cables are impractical or inconvenient, the technology with larger distances between the coils is expected to be incorporated into society. However, more research needs to be done in this area, both in the aspect of improving the technology but also the risk of the electromagnetic fields to affect the human body negatively.

The objective of this project is to wirelessly transfer power to a resistive load, located at a distance of one meter with a desired efficiency of at least 50 %. To fulfill the objective a two-coil model and a four-coil model were analyzed using a frequency of 200kHz. This was done by circuit calculations, simulations in COMSOL Multiphysics<sup>®</sup> and simulations in LTspice. It was decided that the two coil system was sufficient to use, thus it was the only model implemented in practice. The real system was tested with an output power of approximately 20 W by using loads between 5 and 20  $\Omega$ . The achieved efficiency for a 10  $\Omega$  load was 70 % in the simulations and 51 % in the real prototype. The difference was likely caused by a larger voltage drop in the wires than anticipated, a high quality factor, and due to the fact that the magnetic field was affected by surrounding metallic objects in the lab where the experiments were conducted.

Keywords: WPT, IPT, CPT, resonant coupling.



## Acknowledgements

We would like to thank our examintor Yujing Liu for guiding us through this project. We would also like to thank Eva Palmberg for helping us with the analytical calculations. Furthermore, would we like to thank our supervisor Richard Kahl and Josefine Sandahl at Sigma Embedded for their support throughout the project. Not to mention, a very special thank you to Daniel Pehrman who helped us with simulations in LTspice. Last but not least we would like to thank Robert Karlsson for supporting us with all practical details in the lab.

Maria Nisshagen and Emma Sjöstrand, Gothenburg, Sweden  
June 14, 2017



---

## Abbreviations

WPT	Wireless Power Transfer
CPT	Contactless Power Transfer
IPT	Inductive Power Transfer
EMF	Electromagnetic fields
<i>emf</i>	electromotive force
KVL	Kirchoff's Voltage Law
AC	Alternating Current
DC	Direct Current
PF	Power Factor
VA	Volt-Ampere
SS	Serie-Serie
SP	Serie-Parallel
PS	Parallel-Serie
PP	Parallel-Parallel
ESR	Equivalent Series Resistance
PWM	Pulse Width Modulation
RMS	Root Mean Square
FEM	Finite Element Method
CT	Circuit Theory
CMT	Coupled Mode Theory

## Notations

$\vec{H}$	Magnetic field [A/m]
$\vec{J}$	Current density [A/m <sup>2</sup> ]
$\vec{E}$	Electric field [V/m]
<i>emf</i>	Electromotive force [V]
$\vec{B}$	Magnetic flux density [T]
$\Phi$	Magnetic flux [Wb]
$I$	Current [A]
$V$	Voltage [V]
$\mu_0$	Absolute permeability of vacuum ( $\mu_0 = 4\pi * 10^{-7}$ [H/m])
$\mu_r$	Relative permeability
$\mu$	Absolute permeability [H/m]
$C$	Capacitance [F]
$L$	Inductance [H]
$R$	Resistance [ $\Omega$ ]
$M$	Mutual inductance [H]
$N$	Number of turns
$A$	Area of wire [m <sup>2</sup> ]
$l$	Length of wire coil [m]
$k$	Coupling factor
$\eta$	Efficiency [%]

---

$\sigma$	Electrical conductivity [S/m]
$\delta$	Skin depth [m]
$Q$	Quality factor
$\omega$	Angular frequency [rad/s]
$\Delta f$	Bandwidth frequency [Hz]
$c$	Speed of light [m/s]

# Contents

<b>List of Figures</b>	<b>xiii</b>
<b>List of Tables</b>	<b>xv</b>
<b>1 Introduction</b>	<b>1</b>
1.1 Background . . . . .	1
1.2 Aim . . . . .	2
1.3 Objective . . . . .	3
1.4 Method . . . . .	3
1.5 Scope . . . . .	3
<b>2 Theory</b>	<b>5</b>
2.1 Electromagnetic field theory in IPT systems . . . . .	5
2.2 Circuit theory in IPT systems . . . . .	8
2.2.1 Two-coil system . . . . .	8
2.2.2 Four-coil system . . . . .	9
2.3 Resonant coupling . . . . .	10
2.3.1 Two-coil system . . . . .	10
2.3.2 Four-coil system . . . . .	11
2.4 Impedance matching . . . . .	12
2.5 Q-factor . . . . .	12
2.6 Stray capacitance . . . . .	13
2.7 Coil winding . . . . .	13
2.8 Coil resistance . . . . .	14
2.9 Analytical calculation of self inductance . . . . .	15
2.10 Analytical calculation of mutual inductance . . . . .	16
2.11 Compensation capacitors . . . . .	16
2.12 Inverter . . . . .	18
<b>3 Analytical calculations</b>	<b>23</b>
3.1 Two-coil system . . . . .	24
3.2 Four-coil system . . . . .	27
<b>4 Electromagnetic field analysis</b>	<b>31</b>
4.1 Flat coils . . . . .	32
4.2 Solenoid coils . . . . .	32
4.2.1 Q-factors . . . . .	34

4.2.2	Ferrite implementation . . . . .	34
4.2.3	Electromagnetic fields . . . . .	35
4.3	Four-coil system . . . . .	36
<b>5</b>	<b>Electric circuit analysis</b>	<b>39</b>
5.1	Two-coil system . . . . .	40
5.2	Four-coil system . . . . .	41
5.3	Inverter losses . . . . .	43
<b>6</b>	<b>Construction of prototype</b>	<b>45</b>
6.1	Coil design . . . . .	45
6.2	Compensation capacitors . . . . .	46
6.3	Control of inverter . . . . .	48
6.4	Inverter . . . . .	49
6.5	Q-factor . . . . .	51
6.6	Test of resonant ITP system . . . . .	51
<b>7</b>	<b>Environmental and ethical aspects</b>	<b>57</b>
7.1	Health aspects regarding exposure to electromagnetic fields . . . . .	57
7.2	Environmental aspects . . . . .	57
<b>8</b>	<b>Discussion</b>	<b>59</b>
8.1	Areas of opportunity . . . . .	59
8.2	Future work . . . . .	59
8.3	Possible health risks . . . . .	60
8.4	Environmental aspects . . . . .	60
<b>9</b>	<b>Conclusion</b>	<b>63</b>



# List of Figures

2.1	Simplified circuit of an IPT system . . . . .	5
2.2	Two coils linked together by mutual flux $\Phi_{12}$ . . . . .	6
2.3	Two equivalent circuit representations of a two-coil system . . . . .	8
2.4	Two equivalent circuit representations of a four-coil system . . . . .	10
2.5	Serie-Serie compensated topology . . . . .	11
2.6	Mutual inductance of a four-coil system . . . . .	11
2.7	Simplified electrical circuit representation of a IPT system . . . . .	12
2.8	Winding of two coils . . . . .	14
2.9	The skin depth ( $\delta$ ) visualized in a conductor . . . . .	14
2.10	A single loop with cross section radius $r$ and loop radius $a$ . . . . .	15
2.11	Two thin axially aligned loops in air separated by distance $d$ . . . . .	16
2.12	Full circuit representation of a capacitor . . . . .	17
2.13	One-phase inverter . . . . .	19
2.14	Theoretical Voltage output from an inverter . . . . .	20
3.1	Graph showing the mutual inductance in terms of the radius of the coils. . . . .	23
3.2	Fully compensated circuit with two-coil system . . . . .	25
3.3	Fully compensated circuit with four-coil system . . . . .	27
3.4	Efficiency for the two loads with various distance $d_{12}$ and $d_{34}$ . . . . .	28
3.5	Efficiency dependent on the load for a two and four-coil system . . . . .	29
4.1	Two 2D axis symmetric principles . . . . .	31
4.2	The magnetic flux density is relatively strong nearby the primary coil at the top and weak in the receiving coil near the bottom . . . . .	33
4.3	Points where measurements of magnetic field and flux density as well as electric field were performed . . . . .	35
4.4	Magnetic field and flux and electric field nearby the coils . . . . .	36
4.5	Principal sketch of a four-coil system simulated in COMSOL . . . . .	37
5.1	One-phase full bridge inverter simulated in LTspice . . . . .	39
5.2	The resonant circuits of the two-coil system . . . . .	40
5.3	Simulated waveforms with a two-coil system . . . . .	40
5.4	One-phase inverter together with the resonant circuits of the four-coil system . . . . .	41
5.5	Simulated waveforms with a four-coil system . . . . .	42
5.6	Switching waveforms from which the inverter losses are estimated . . . . .	43

6.1	Sending and receiving coil seen from above . . . . .	46
6.2	Capacitors on the primary and secondary side . . . . .	47
6.3	Waveforms from the microcontroller into the inverter . . . . .	48
6.4	Simplified graphics of the inverter . . . . .	49
6.5	Voltage out from physical inverter together with simulated voltage . .	50
6.6	View of the inverter using normal and heat camera . . . . .	50
6.7	The entire test setup as it looked in the lab . . . . .	51
6.8	Comparison between simulated and measured voltage and current over the load . . . . .	52
6.9	Graph showing the efficiency of the system with simulations and mea- surements at different loads . . . . .	53
6.10	Comparison between simulated and measured voltage and current over the load with AC-resistance in the coils . . . . .	54
6.11	Efficiency graph with the resistance of the coils simulated with AC resistance . . . . .	55
6.12	Heatings measured in the primary circuit . . . . .	55

# List of Tables

2.1	Conductivity of some common materials used in conductors . . . . .	14
2.2	Some characteristics of different capacitor types . . . . .	17
3.1	Calculated mutual inductance for single loops in air . . . . .	24
3.2	Calculated and known parameters . . . . .	25
3.3	$N_1$ and $N_1$ varied to evaluate voltage, current, and efficiency with a 5 $\Omega$ load . . . . .	25
3.4	$N_1$ and $N_1$ varied to evaluate voltage, current, and efficiency with a 20 $\Omega$ load . . . . .	26
3.5	Calculated parameters . . . . .	26
3.6	Calculated bandwidth and Q-factors . . . . .	26
3.7	Calculated and known parameters of the four-coil system . . . . .	28
3.8	RMS current and voltage in primary and receiving circuit with a 5 $\Omega$ load . . . . .	29
3.9	RMS current and voltage in primary and receiving circuit with a 20 $\Omega$ load . . . . .	29
4.1	Simulated inductances using flat coils in Comsol . . . . .	32
4.2	Simulated inductances using solenoid coils in COMSOL . . . . .	33
4.3	Calculated and simulated bandwidth and Q-factor . . . . .	34
4.4	Couplings factor with different use of ferrite ( $\sigma = 0.5[S/m]$ and $\mu =$ 2000) . . . . .	34
4.5	Simulated inductances for the four-coil system . . . . .	37
4.6	Mutual inductance with a 5 $\Omega$ load and distance $d_{12}=d_{34}=0.35$ m . .	37
4.7	Mutual inductance with a 20 $\Omega$ load and distance $d_{12}=d_{34}=0.2$ m . .	38
5.1	Rms current and voltage in primary and receiving circuit with a 5 $\Omega$ load using two-coil system . . . . .	41
5.2	RMS current and voltage in primary and receiving circuit with a 20 $\Omega$ load using two-coil system . . . . .	41
5.3	RMS current and voltage in primary and receiving circuit with a 5 $\Omega$ load using four-coil system . . . . .	42
5.4	RMS current and voltage in primary and receiving circuit with a 20 $\Omega$ load using four-coil system . . . . .	43
6.1	Simulated inductances compared with measured values . . . . .	46
6.2	Simulated and measured bandwidth and Q-factor . . . . .	51

6.3	The four methods to measure the power on the secondary side . . . .	52
6.4	RMS values of current through the load and voltage over the load . .	53
6.5	Efficiency comparison with $7\ \Omega$ . . . . .	54
6.6	Efficiency measurements with increasing power input . . . . .	56
7.1	Reference values for fields with frequency ( $f$ ) between 3 kHz and 10 MHz . . . . .	57

# 1

## Introduction

### 1.1 Background

Wireless power transfer (WPT) is the transmission of energy from a source to an electrical load over an air gap without using physical contact [1]. This technology was first experimented with during the late 19th century by Nicolas Tesla, who managed to create several different WPT technologies [2]. WPT can be classified today into three categories: radiative, non-radiative capacitive coupling, and non-radiative magnetic coupling [3].

Radiative and non-radiative capacitive coupling are not convenient to use when it comes to transfer relatively large power. Radiative WPT, such as microwave or laser, uses electromagnetic radiation for far-field transmission. However, due to its omnidirectional character the efficiency is very low, thus more useful to transmit information rather than power [3, 4]. Non-radiative capacitive coupling WPT uses an electric field from a capacitive coupling for near-field transmission. This technology is not often used because high voltages are required to transfer any significant amount of power and the intensity of the electric field can harm the human body [3].

With non-radiative magnetic coupling WPT it is possible to transfer a great deal of power. Non-radiative magnetic coupling is a near-field transmission technology which uses a magnetic field to transfer power over an air gap [3]. Transformers, electrical machines, and wireless charges are electrical devices that make use of magnetic coupling WPT, which is often referred to as contactless power transfer (CPT) or inductive power transfer (IPT).

One of the most common magnetic coupling WPT is the resonant IPT. The resonant IPT is similar to using transformers but the coils are connected to capacitors in different topologies in order to create resonance (typically between 20 kHz and a few MHz). This makes the circuit as seen from the source completely resistive, thus the source does not have to supply reactive power from the large leakage inductance [4]. Sometimes the coils are not connected to capacitors but instead designed to self resonate.

IPT development has increased rapidly during the last couple of years. This covers a wide range of applications from charging or powering electrical vehicles, medical implants, wireless sensors, laptops, and mobile phones. It is necessary to use IPT

where cables are impractical, due to safety reasons or inconvenience. An example is in workshops or coalmines where there would be less chance of explosion from a spark caused by friction on wires. Also it is convenient where cables are exposed to harsh environments such as under water, cold temperatures, chemicals etc [5]. Sometimes it is even used because there are no other possible solution to transfer power to a location, for example in some chemical labs [1].

Smaller IPT devices such as mobile phones chargers have an efficiency above 70 %, while chargers for electrical cars have efficiencies greater than 90 %. However, the air gaps of these applications ranges from a few mm to about 300 mm [4]. Since the use of electrical equipment increases, it is possible to assume that the need of being able to power these devices will also increase, thus also making it more convenient for the users to expand the wireless power range.

A great deal of research is being carried out around the globe on this subject. Massachusetts Institute of Technology (MIT) is one of researchers who managed to transfer power over a distance of two meters to power a light bulb with an efficiency of around 40 % already in 2007. Since then many other projects have managed to transfer more power over longer distances. In 2016 a group of researchers from Korea Advanced Institute of Science and Technology (KAIST) was able to transfer 10 W over a distance of seven meters.

However, long distance inductive power transfer is still not economical enough for commercial purposes due to complex and bulky designs [6]. Installation cost is much higher than conventional systems and IPT systems have lower efficiency than a transformer. Other challenges are losses caused by fast switching power electronics, difficulties in modeling of switch mode nonlinear circuits, stability control, and variable frequency controlled systems. Thus more research is necessary before this technology can enter the market.

Other research that is necessary before the technology can enter the market is the impact it will have on humans and the environment. Rapid increase of atmospheric temperature, melting ice, ozone destruction, forest degradation, and pollution are examples of what human inventions can cause. Therefore it is important to consider environmental and ethical aspects. For example, the maximum magnetic field the general public is allowed to be exposed to is  $27 \mu\text{T}$  in the frequency range 3-10000 kHz [7]. Another example is the high switching frequency in the inverter, which can cause EMF emission [3].

## 1.2 Aim

The aim of the project is to wirelessly transfer power to a resistive load, e.g. a lamp, located one meter away by means of resonant coils with a desired efficiency of at least 50 %.

## 1.3 Objective

- Investigate how different topologies and setups affect resonant IPT
- Create a model in Comsol Multiphysics and LTspice
- Implement and compare one of the simulations with a physical design
- Investigate the environmental and ethical aspects of IPT

## 1.4 Method

In order to get a basic understanding about inductive power transfer systems research articles, books and reports about IPT were gathered from Chalmers' library and data bases available at Chalmers' online library. A literature study regarding ethical and environmental aspects was also conducted based on studies and reports from these data bases.

Calculations were done in order to get desired current and voltage of the load. When the desired values of the components were decided a simulation model was created in COMSOL Multiphysics® in order to analyze the magnetic field and decide the final geometry of the coils needed in the IPT system. With the LTspice model it was possible to study the current/voltage waveforms and easily analyze any changes in the system, when frequency, coupling factor or converter parameters were changed.

When the simulations were satisfying components were selected and ordered. While waiting for the components to arrive a microcontroller was programmed to achieve the desired frequency of the system. Once all the components were available, a prototype was assembled and measurements were conducted in order to verify that everything was working properly and within specifications. After that the circuit was tested and compared with the simulated designs.

## 1.5 Scope

In order to finish the project within the time frame, some aspects were not considered in the design. Trade-offs regarding efficiency, robustness and cost were not treated thoroughly. Due to relatively large distance between the coils, misalignment was not investigated. Overload communication on the inductive coupling and control of when the coils are within reach were not investigated either. Frequency control and bifurcation was not investigated. Complex transformer design to reduce stray capacitance was not looked into either.





# 2

## Theory

When dealing with non-radiative magnetic power transfer, the system is classified to be either near-range or mid-range. By definition mid-range is when the distance between the coils is larger than the coil dimensions, and near-range is defined as a system with a distance between coils smaller than the coil dimensions [3]. Hence, in this report, the region between near-range and mid-range is when the coil dimension and the air gap is the same size.

An IPT system consisting of two coils is made up by a primary rectifier, an inverter, a primary coil, a secondary coil, and a secondary rectifier [3]. The primary rectifier, the inverter, and the primary coil together are called the transmitter. The secondary coil and the secondary rectifier makes up the receiver. Since the load in this project is purely resistive the rectifier on the secondary side is not necessary. A simplified circuit is shown in Figure 2.1.

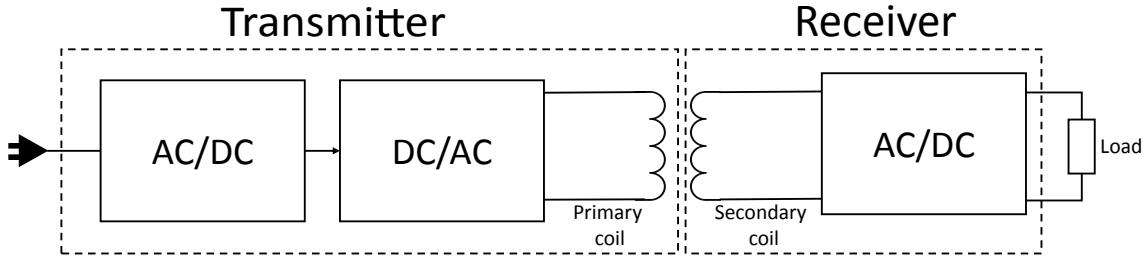


**Figure 2.1:** Simplified circuit of an IPT system

It is possible to use multiple coils instead of two coils. Generally in this case, four coils are used. The advantage of using four coil system is that it is possible to tune the circuit to achieve higher efficiency [3]. This is explained more in Section 2.2.2.

In this chapter, all the components that will be assembled in the IPT system will be explained. In order to understand how power is transferred inductively a basic theory regarding electromagnetic is presented. Furthermore, circuit theory, resonant IPT, and resonant phenomena are described.

### 2.1 Electromagnetic field theory in IPT systems

To mathematically describe how power inductively is transmitted mainly two laws are used; Ampere's circuit law and Faraday's law of induction. Ampere's circuit law

describes that a changing magnetic field intensity around a closed loop  $L$ , is equal to the electric current passing through the surface bounded by the loop. This is given by

$$\nabla \times \vec{H} = \vec{J} \Leftrightarrow \oint_L \vec{H} \cdot d\vec{l} = \int_S \vec{J} \cdot d\vec{s} = I_{encl} \quad (2.1)$$

where  $\vec{J}$  is the current density [A/m<sup>2</sup>],  $I_{encl}$  [A] is the current enclosed in the circuit and  $\vec{H}$  [A/m] is the magnetic field [8]. Faraday's law of induction states that a time changing magnetic field gives rise to an electromotive force (*emf*). The general form of Faraday's law is given by

$$\nabla \times \vec{E} = -\frac{\partial \vec{B}}{\partial t} \Leftrightarrow \oint_L \vec{E} \cdot d\vec{l} = -\frac{d}{dt} \int_S \vec{B} dA = emf \quad (2.2)$$

where  $\vec{E}$  [V/m] is the electric field,  $\vec{B}$  [T] is the magnetic flux density and  $A$  [m<sup>2</sup>] is the area enclosed by the loop [8]. By combining Faraday's law of induction with the mathematical expression of magnetic flux  $\Phi$  given by

$$\Phi = \int_S B dA \quad (2.3)$$

it can be observed that the electromotive force *emf* is proportional to the derivative of the magnetic flux [8]. By applying Lenz's law, which explains that the induced *emf* causes a current to flow in a direction to oppose change in the magnetic field, the equation can be written as

$$emf = -\frac{d\Phi}{dt} \quad (2.4)$$

If two coils are linked together via a magnetic field they are said to have a mutual flux  $\Phi_{12}$ . Thus, if a current  $I_1$  flows through one of the coils, it creates magnetic flux which induce *emf* in the second coil. This allows a current  $I_2$  to flow in the coil if the circuit, in which the coil is positioned, is closed [8]. This is illustrated in Figure 2.2.

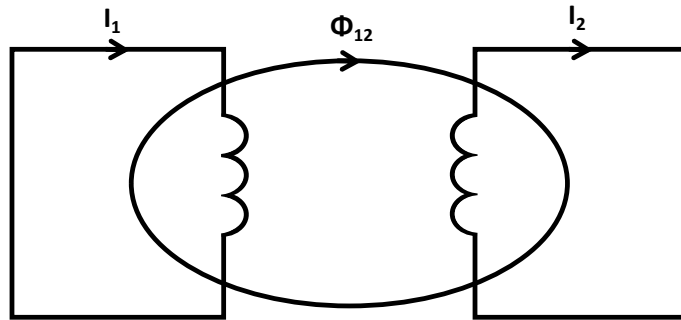


**Figure 2.2:** Two coils linked together by mutual flux  $\Phi_{12}$

When *emf* is induced in nearby coils, it is also said to be induced magnetically by a mutual inductance  $M$ . The mutual inductance changes depending on how the coils are positioned to each other. If there is a small distance between the coupled coils, more magnetic flux interacts with the nearby coils and induce a larger *emf*. Since

the magnetic field is directly proportional to the current flux must also be directly proportional to the current [8]. Hence, the mutual inductance is related to magnetic flux as

$$M_{12} = \frac{N_1 \Phi_{12}}{I_2} \quad (2.5)$$

where  $N_1$  is number of turns on the primary coil and  $I_2$  is current induced in the secondary coil. Note that the mutual inductance  $M_{12}$  is equal to  $M_{21}$  which is calculated in the same manner but using the secondary turn  $N_2$  and the primary current  $I_1$  instead [8]. The mutual inductance can also be calculated by

$$M_{12} = \frac{V_2}{I_1 \omega} \quad (2.6)$$

where  $V_2$  is the voltage over the secondary coil and  $\omega$  is the operational frequency [rad/s]. Mutual inductance can be increased by increasing the size of the coils or increasing the flux through the coupled coils. This can be done by placing the windings on a common iron core which directs the magnetic flux [8].

This is however not practical to use in IPT applications. Instead it may be more useful to increase magnetic flux through the coupled coils by using separate ferrite cores. Ferrite is a material made of mainly iron. It is commonly used in high frequency IPT application due to its' well suited magnetic properties [9].

Electromagnetic force *emf* created within the conductor due to the changing magnetic field around its' own turns is called self-inductance. Self inductance can be calculated similarly as mutual inductance by

$$L = \frac{N_1 \Phi_1}{I_1} \quad (2.7)$$

where  $\Phi_1$  is the flux through the primary coil. Likewise, the self inductance can also be calculated as

$$L = \frac{V_1}{I_1 \omega} \quad (2.8)$$

The mutual inductance is related to the self inductance by means of coupling coefficient  $k$  given by

$$k = \frac{M}{\sqrt{L_1 L_2}} \quad (2.9)$$

where  $L_1$  is the self-inductance in the primary coil and  $L_2$  is the self-inductance in the secondary coil. If  $k = 1$  the coils are perfectly coupled, if  $k$  is bigger than 0.5 the coils are said to be tightly coupled and if  $k$  is smaller than 0.5 the coils are said to be loosely coupled.

When the coils are not perfectly coupled some flux will not interact with the secondary coil. This is called leakage flux. The leakage flux will store and discharge

magnetic energy, acting as an inductor, which is called leakage inductance [8]. The leakage inductance can be calculated as

$$L_{leakage} = L_{selfinductance} - M \quad (2.10)$$

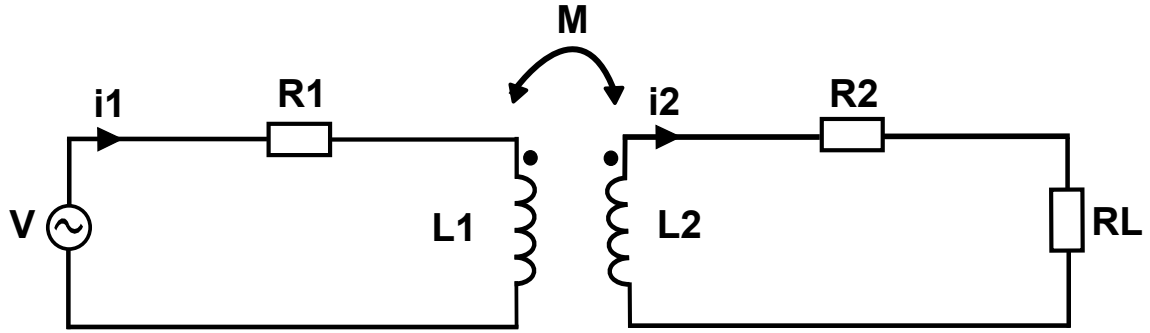
## 2.2 Circuit theory in IPT systems

Circuit theory is, as the name implies, used to analyze the circuits used in IPT systems. In this project a two-coil system and a four-coil system is evaluated mainly by means of equivalent models and Kirchhoff's voltage law (KVL).

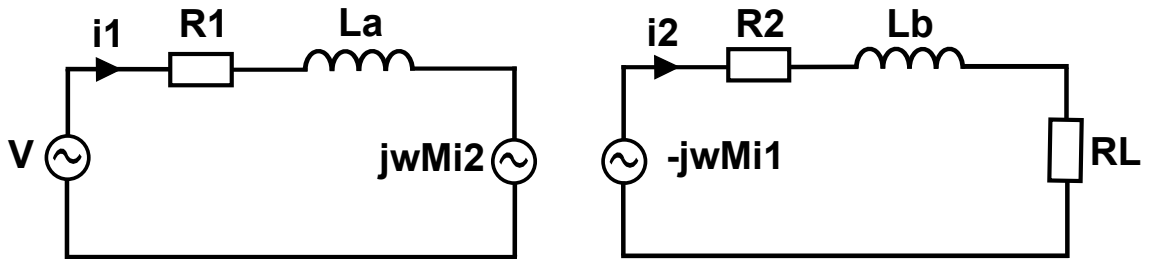
### 2.2.1 Two-coil system

The two-coil IPT system can be represented as an AC source together with an inductance on the primary side and a load and inductance on the secondary side, which can be seen in Figure 2.3a.  $R_1$  and  $R_2$  represents the resistance in the wires and  $L_1$  and  $L_2$  represents the self inductances.  $R_L$  is the resistive load.

An equivalent model is shown in Figure 2.3b where the induced *emf* on the primary side is represented by a voltage source equal to  $j\omega Mi_2$  [10]. Likewise the induced *emf* on the secondary side is equal to  $j\omega Mi_1$ .  $L_a$  and  $L_b$  represent the leakage inductances on the primary and secondary side respectively.



(a) Electric circuit representation of the IPT system



(b) Electric circuit representation of IPT system with induced voltage

**Figure 2.3:** Two equivalent circuit representations of a two-coil system

To calculate the electric circuit parameters Kirschoff's voltage law (KVL) is used.

The following equations were derived from KVL on both the primary side and the secondary side.

$$V - i_1 R_1 - i_1 j\omega L_a - j\omega M i_2 = 0 \quad (2.11)$$

$$- j\omega M i_1 - i_2 R_2 - i_2 j\omega L_b - i_2 R_L = 0 \quad (2.12)$$

where  $\omega$  is the resonance frequency of the system [11]. The efficiency can be derived from the circuits in Figure in 2.3 to

$$eff = \frac{R_L}{(R_L + R_2) + (1 + \frac{R_1(R_2 + R_L)}{\omega^2 M^2}) + R_1(\frac{L_2}{M})^2} \quad (2.13)$$

It can be noted that if a high frequency is used, the system will have higher efficiency.

### 2.2.2 Four-coil system

The four-coil system consists of a source coil ( $L_1$ ), a sending coil ( $L_2$ ), a receiving coil ( $L_3$ ) and a load coil ( $L_4$ ). The source coil and the sending coil should be closely coupled as should the receiving coil and the load coil. The system is modelled by taking all mutual inductance between all four coils in account ( $M_{12}$ ,  $M_{13}$ ,  $M_{14}$ ,  $M_{23}$ ,  $M_{24}$ ,  $M_{34}$ ). However, often it is desirable to simplify the model which is done by only taking  $M_{12}$ ,  $M_{34}$  and  $M_{23}$  into account, which can be seen in Figure 2.4a. Similarly as in the two-coil system an equivalent model, shown in Figure 2.4b can be derived. From this KVL gives

$$V - i_1 R_1 - j\omega L_a - V_{12} = 0 \quad (2.14)$$

$$V_{21} - i_2 R_2 - j\omega L_b - V_{23} = 0 \quad (2.15)$$

$$V_{32} - i_3 R_3 - j\omega L_c - V_{34} = 0 \quad (2.16)$$

$$V_{43} - i_4 R_4 - j\omega L_d - i_4 R_L = 0 \quad (2.17)$$

where  $V_{12}$  equal to  $j\omega M_{12}i_2$ ,  $V_{21}$  equal to  $-j\omega M_{21}i_1$ ,  $V_{23}$  equal to  $j\omega M_{23}i_3$ ,  $V_{32}$  equal to  $-j\omega M_{32}i_2$ ,  $V_{34}$  equal to  $j\omega M_{34}i_4$ ,  $V_{43}$  equal to  $-j\omega M_{43}i_3$  [12].

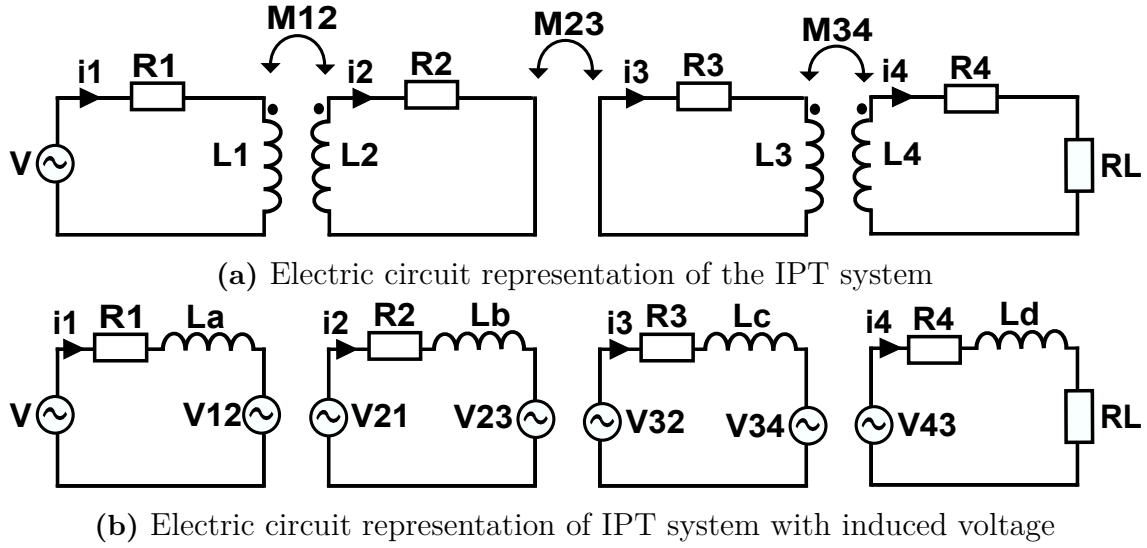


**Figure 2.4:** Two equivalent circuit representations of a four-coil system

## 2.3 Resonant coupling

In mid-range IPT systems the coupling between the sending and receiving side is poor, due to the long distance between the coils. To get good power transfer efficiency high frequency is needed. However, when using high frequency the system impedance as seen by the source becomes more and more inductive, thus making the power factor (PF) smaller and smaller (voltage and current more out of phase). This means that more reactive power circulates in the system, hence the inverter needs high VA rating. The circulating reactive power also decreases power transfer.

To get better power transfer capability and to decrease the size of the inverter, capacitive compensation is needed [1]. As a consequence the impedance as seen by the source becomes purely resistive. In other words, resonant coupling takes advantage of resonance of inductance and capacitance in a LC tank to compensate for the leakage inductance [4]. The compensation could either be done by adding capacitors to the circuit or letting the coils resonate at its' own resonance frequency. It has been seen that two systems that resonates at the same frequency, exchange power efficiently [13], therefore it is beneficial if the sending and the receiving side resonates at the same frequency. The capacitance is chosen such that it cancels out the inductance, specifically it is calculated by

$$\omega = \frac{1}{\sqrt{LC}} \quad (2.18)$$

### 2.3.1 Two-coil system

The four most common topologies in a two-coil system are: Series-Series (SS), Series-Parallel (SP), Parallel-Series (PS), and Parallel-Parallel (PP), where the series or parallel refers to how the capacitors should be placed in relation to each other on

the primary side and the secondary side [3].

General SS compensated IPT system has two advantages. The compensation capacitors on both primary and secondary side are independent of the load and the mutual inductance. Reflected impedance on secondary winding only has a real component, thus it will only draw active power [1]. The SS topology is shown in Figure 2.5.

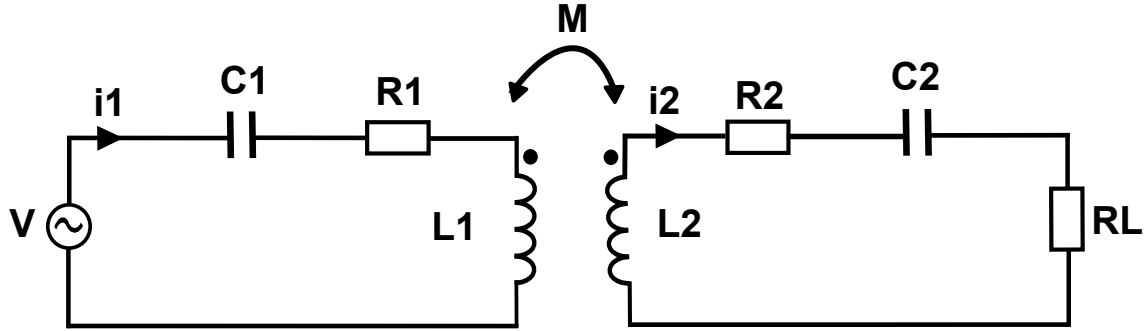


**Figure 2.5:** Serie-Series compensated topology

### 2.3.2 Four-coil system

The sending coil and the receiving coil circuit in the four coil system are often closed with their own stray capacitance. In many systems the source impedance is much larger than the resistance of the source coils, thus making it negligible. The same thing for the load side. In the sending and the receiving coil there are both ohmic losses and radiation losses. However, when talking about long distance power transfer the radiation losses are small [14].

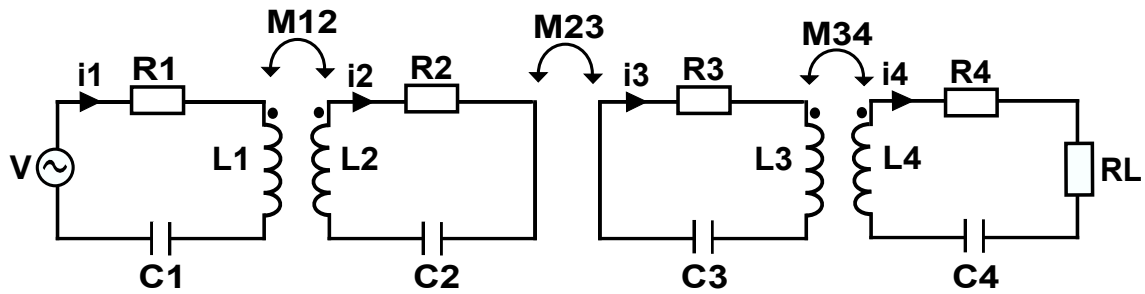


**Figure 2.6:** Mutual inductance of a four-coil system

In a four-coil system, the source coil is often just one single loop coil. To this a capacitance is added to resonate at the desired frequency. The sending coil is a multiturn coil which is often built in such a way that it will resonate with its own capacitance at the desired frequency. The receiving side is defined similarly. Normally the coupling factor  $k_{12}$  is fixed to the same value as  $k_{34}$  [15].

## 2.4 Impedance matching

An IPT system can also be represented by a source impedance and a load impedance, visualized in Figure 2.7. Maximum power transfer occurs when the source impedance and the load impedance equal each other ( $R_s = R_l$  and  $X_s = -X_l$ ). This is called impedance matching [4].

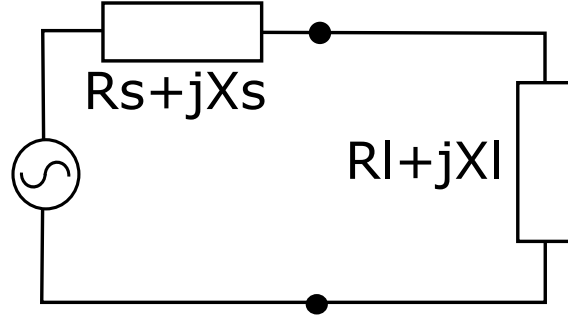


**Figure 2.7:** Simplified electrical circuit representation of a IPT system

The efficiency of the system when the circuits are compensated can be derived as

$$\eta = \frac{R_l}{R_s + R_l} \quad (2.19)$$

Thus, when the impedance matching condition is fulfilled the efficiency is equal to 50 %. It can be seen that if  $R_l > R_s$  the efficiency will increase. This is used in the four-coil system by adjusting the distance between coil 1 and 2, and coil 3 and 4. By doing this the coupling factors between the four coils change which affects the impedance of the system. Thus the distances can be varied to achieve maximum efficiency [15].

## 2.5 Q-factor

The Q-factor (quality factor) is a dimensionless parameter used to tell how efficient a system oscillates. A high Q-factor indicates that the oscillations goes further with more energy, while a low Q-factor make the oscillation attenuate faster. When a high Q-factor is achieved, the frequency has to be close to the actual resonant frequency (smaller bandwidth). Thus a high Q-factor has more energy but is more difficult to tune [1]. The primary Q-factor is calculated as

$$Q_1 = \frac{(L_a + M)R_L}{\omega_0 M^2} \quad (2.20)$$

where  $L_a$  is the primary leakage inductance,  $M$  is the mutual inductance,  $R_L$  is the load and  $\omega_0$  is the resonance frequency. The Q-factor of the receiving side is calculated as

$$Q_2 = \frac{\omega_0(L_b + M)}{R_L} \quad (2.21)$$



The Q-factor can also be determined by  $Q = \frac{f_0}{\Delta f}$ , where  $f_0$  is the mid-resonance frequency and  $\Delta f$  is the bandwidth, at which resonance occurs. A loosely coupled system will have a narrow bandwidth.

## 2.6 Stray capacitance

A coil can be seen as a resistance, to model the winding losses, in series with an ideal inductance, at really low frequencies. However, at high frequencies the coil wire can be represented as a long transmission line with small inductances and stray capacitances distributed along the line [13]. The total capacitance of the coil is referred to as parasitic capacitance or stray capacitance. This is important to consider when designing the coils, since high frequency is desired in IPT systems. If the chosen frequency is too high, the coil can become more capacitive than inductive. The stray capacitance of a straight wire can be calculated by first calculating the self resonance frequency as

$$f_{self} = \frac{v}{2l} \quad (2.22)$$

where  $v$  is the velocity at which the wave propagates through the wire and  $l$  is the length of the wire. Thereafter, the capacitance of a straight wire can be calculated by using Equation 2.18 [16].

It is difficult to analytically calculate the stray capacitance of a coil. There are some methods used to calculate stray capacitance such as numerical methods, analytical methods, and methods based on laboratory measurements [17]. To analytically calculate the stray capacitance of a coil is, however, out of scope for this project.

## 2.7 Coil winding

There are mainly two ways to design a coil in a resonant IPT system. One is to turn the wire outwards in a flat, spiral direction. This coil is sometimes referred to as spiral or pancake coil. In this report it is called flat coil. In the second coil the wire turns upwards into a helix, or a solenoid shape. In this report it is referred to as solenoid coil. The two types can be seen in Figure 2.8. There are more complex coil designs which are used to reduce stray capacitance [17]. However, that is outside the scope of this project.

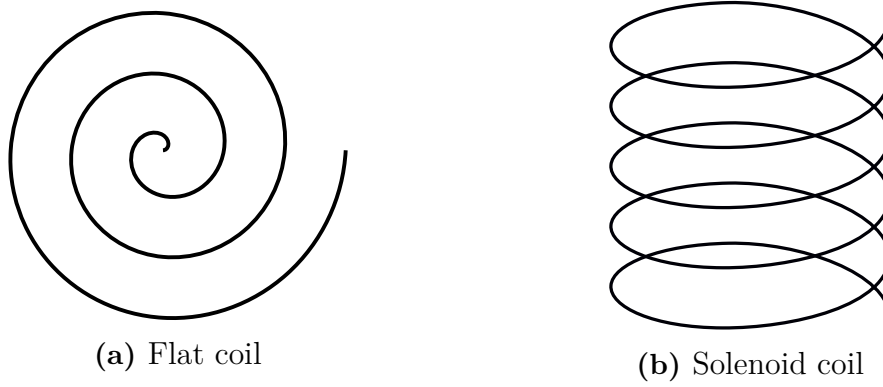


**Figure 2.8:** Winding of two coils

## 2.8 Coil resistance

The DC resistance  $[\Omega]$  of a conductor depends on wire length, wire area and electrical conductivity of the material. It is calculated by

$$R_{DC} = \frac{l}{\sigma A} \quad (2.23)$$

where  $\sigma$  is the electrical conductivity  $[\text{S/m}]$  of the material used in the wire,  $l$  is the length of the wire  $[\text{m}]$ , and  $A$  is the area of the wire  $[\text{m}^2]$  [8]. To get low resistance in the coils the electrical conductivity of the material  $\sigma$  needs to be high. Table 2.1 lists the conductivity of some common materials [8].

**Table 2.1:** Conductivity of some common materials used in conductors

Material	Conductivity, $\sigma$ $[\text{S/m}]$
Copper	$5.8 \cdot 10^7$
Aluminium	$3.54 \cdot 10^7$
Iron	$1 \cdot 10^7$

At high frequency AC applications the main resistance comes from skin effect which makes the current press towards the edges of the conductor which create a smaller effective area. This is visualized in Figure 2.9.

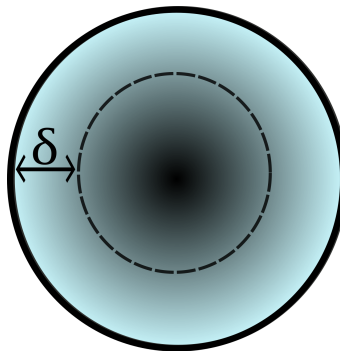


**Figure 2.9:** The skin depth ( $\delta$ ) visualized in a conductor

The skin depth,  $\delta$ , defines the area where the current flows and is calculated by

$$\delta = \frac{1}{\sqrt{\pi f \mu \sigma}} \quad (2.24)$$

where  $\mu$  is the permeability of the used material in the wire,  $f$  is the frequency [Hz], and  $\sigma$  is, as previously mentioned, the conductivity of the material [S/m].

When the frequency increases, the skin depth decreases. The most common way to get around this is to use a litz wire that consists of multiple, thin strands. The number of strands and the thickness of each strand depends on how much current and at which frequency the system is designed for[8]. The total resistance of the coil can be calculated according to

$$R = \frac{l}{\sigma A} \left[ \frac{1}{4} + \frac{r_{wire}}{2\delta} \right] \quad (2.25)$$

## 2.9 Analytical calculation of self inductance

For a single circular loop in vacuum the total self inductance consists of inner inductance ( $L_{inner}$ ) [H] and outer inductance ( $L_{outer}$ ) [H]. The inner inductance comes from the magnetic field inside of the conductor and is calculated by

$$L_{inner} = \mu_0 \frac{a}{4} \quad (2.26)$$

where  $\mu_0$  is the absolute permeability of vacuum and  $a$  is the coil radius [m]. However, due to the skin effect  $L_{inner}$  approaches zero at high frequencies. In Figure 2.10 the geometry for a single loop with coil radius  $a$  and wire radius  $r$  can be observed.

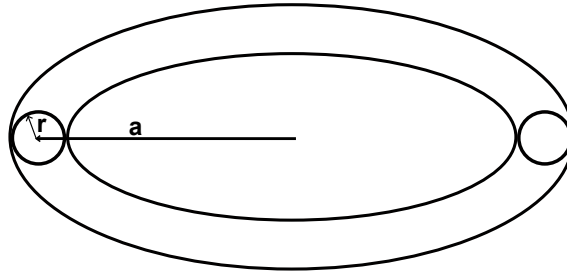


**Figure 2.10:** A single loop with cross section radius  $r$  and loop radius  $a$

The outer inductance comes from the outer magnetic field induced by the current inside the conductor. The outer inductance is calculated by

$$L_{outer} = \mu_0 \frac{2a - r}{2} [(2 - m)K(m) - 2E(m)] \quad (2.27)$$

where  $K(m)$  and  $E(m)$  are complete elliptic integrals [18],  $r$  is the wire radius [m] and  $m$  can be calculated by

$$m = \frac{4a(a - r)}{(2a - r)^2} \quad (2.28)$$

$L_0$  is derived by adding  $L_{inner}$  to  $L_{outer}$ . The total inductance for a coil is achieved by multiplying with  $N^2$  [18]. Thus the self inductance becomes

$$L = L_0 N^2 = (L_{inner} + L_{outer}) N^2 \quad (2.29)$$

## 2.10 Analytical calculation of mutual inductance

The mutual inductance of two coils can be calculated by using elliptic integrals. Mutual inductance can be calculated by

$$M_0 = \mu_0 \frac{\sqrt{ab}}{\sqrt{m}} [(2 - m)K(m) - 2E(m)] \quad (2.30)$$

where  $K(m)$  and  $E(m)$  are the elliptic integrals,  $a$  is the sending coil radius [m],  $b$  is the receiving coil radius [m], and  $m$  is calculated by

$$m = \frac{4ab}{(a + b)^2 + d^2} \quad (2.31)$$

where  $d$  is the distance [m] of the air gap between the midpoint of the coils seen in Figure 2.11

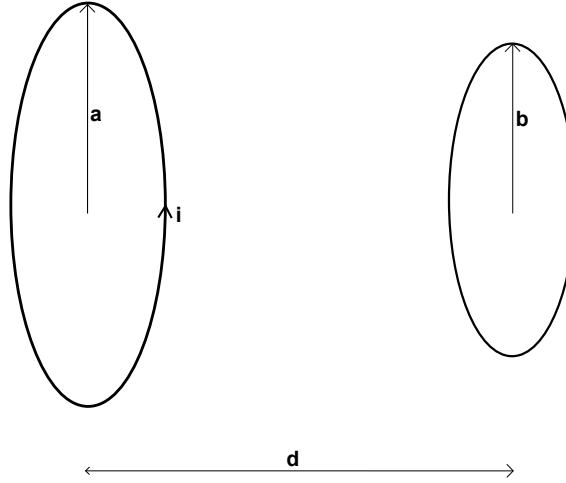


**Figure 2.11:** Two thin axially aligned loops in air separated by distance  $d$

If the coils consist of more than a single turn the mutual inductance is calculated by multiplying  $M_0$  with  $N_1$  and  $N_2$  [18]. Thus the mutual inductance becomes

$$M = M_0 N_1 N_2 \quad (2.32)$$

## 2.11 Compensation capacitors

A capacitor consists of isolated material (dielectric) in between two electrodes, which can be modelled as a capacitor in parallel and series with two resistances and an

inductance as seen in Figure 2.12. The parallel capacitance  $C_p$  [F] models the dielectric resistance,  $L_s$  [H] models the inductance in the connection together with the electrodes and the series resistance  $R_s$  [ $\Omega$ ] models the connections together with the electrodes 2.2.

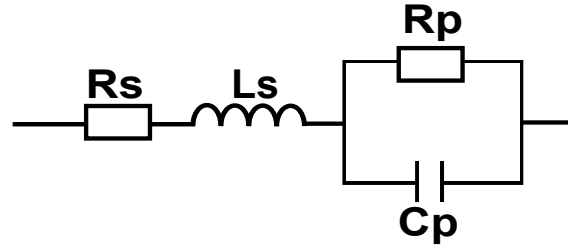


**Figure 2.12:** Full circuit representation of a capacitor

The parallel and series resistance is often modelled together as an equivalent series resistance (ESR), which is dependent on frequency and temperature. ESR is an indicator of all losses in the capacitor, therefore, in many applications it is desirable to keep ESR at a low value.  $R_p$  [ $\Omega$ ] in the dielectric is not infinitely big but has a small current that goes through it. This is called leakage current and can make the capacitors discharge on its own, which is important to consider in some applications [19].

Rate of voltage change is also a parameter important to consider. It decides how fast a capacitor can charge and discharge. If the voltage derivative increases the current through the capacitors will increase which will lead to more losses. This will lead to rise in temperature which increases the resistance. This will result in even greater losses. When the current is too high the electrodes start to evaporate until the pressure is too high and the capacitor breaks. Therefore, it is important to ensure the capacitors can handle enough voltage variations [19].

The dielectric, ESR, and leakage current are frequency, voltage, and temperature dependent. Consequently it can be important to analyze these for different types of capacitors before choosing an appropriate one. There are several different types of capacitor available today but mainly five types; electrolyte, plastic film, ceramic, mica, and double-layer. Some characteristics of those capacitors have been summarized in Table 2.2.

**Table 2.2:** Some characteristics of different capacitor types

Type of capacitor	Frequency	ESR	Stability	Cost
Electrolyte	Low	Low	Middle	Low
Plastic film	High	Low	Middle	Low
Ceramics	High	Low	Middle	Low
Mica	High	Low	High	High
Super capacitor	Low	High	Low	High

In electrolyte capacitors the electrodes are made up of either wet aluminum, dry aluminum or tantalum. ESR and leakage current for wet electrolytes is relatively high and they are very temperature dependent. They are manufactured for  $0.1\ \mu\text{F}$  -  $0.5\ \text{F}$ . The dry type has lower resistance and is manufactured in the interval  $0.1\ \mu\text{F}$  -  $2200\ \mu\text{F}$ . Tantalum has much lower ESR but it is easily short circuited and can start to burn. Generally electrolytes are polarized capacitors that are suitable for low frequencies and filter ripple for DC applications.

Plastic films, also known as polymer films, are unpolarized capacitors manufactured in the interval  $10\ \text{pF}$ - $100\ \mu\text{F}$ , which are more suitable for higher frequencies than electrolytes. There are several different types of polymer films; polyester (PET), polycarbonate (PC), polypropylene (PP), polystyrene and Polyphenylene sulfide (PPS). They all have different pros and cons but generally they have low  $R_s$  and high  $R_p$  which results in low losses and low leakage current.

Ceramics are divided into three categories; class 1, class 2, and class 3. Class 1 is not sensitive to temperature or frequency changes and has low losses. This one is often used for high frequency and oscillation application. Class 2 is more sensitive but still has low losses. Class 3 is more sensitive to changes and can not withstand as much voltage as class 1 and 2. Ceramics can also be built as multilayer. Generally ceramics are unpolarized manufactured in interval  $0.5\ \text{pF}$  -  $100\ \mu\text{F}$  and are suitable for high frequencies.

Mica capacitors are built like multilayer ceramics but uses silver as dielectric. It has low losses and is not sensitive to voltage, temperature or frequency variations. They are manufactured in the interval  $1\ \text{pF}$  -  $0.1\ \mu\text{F}$ . They are, however, expensive.

An electric double-layer capacitor, also known as super capacitor or gold cap, is a mix between a battery and a capacitor. It has very high ESR which limits the discharge rate. It is unpolarized and has high temperature dependence. They are manufactured in the interval  $10\ \text{mF}$  -  $22\ \text{F}$  and is often used as an voltage backup or energy storage [19].

### 2.12 Inverter

A single phase full bridge inverter converts DC voltage to AC voltage by means of four controllable switches. The switches are placed in a bridge with two legs, where each leg consists of two switches and antiparallel diodes, which allows current to go in both directions. The inverter circuit can be seen in Figure 2.13.

The controllable switches are transistors such as BJTs, MOSFETs, GTOs and IGBTs which are controlled by different types of control signals depending on application. The switches can be controlled in mainly three ways; pulse-width-modulated (PWM) mode, square wave mode or single phase voltage cancellation mode.

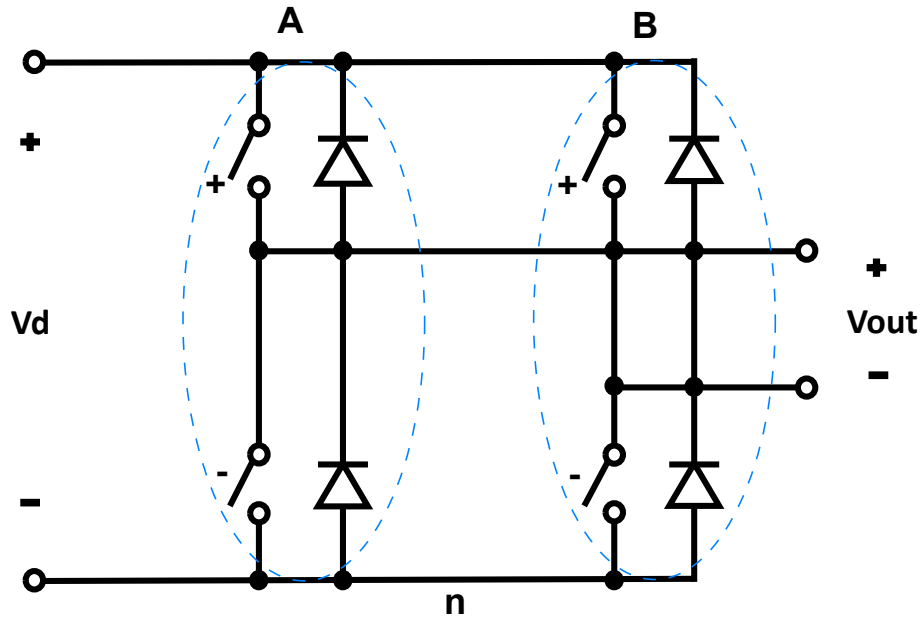


Figure 2.13: One-phase inverter

In PWM a triangular waveform is compared with sinusoidal control voltage to regulate the switches in pairs. When the control voltage is bigger than the triangular waveform one of the pairs is turned on. By changing the duty cycles the output voltage can be controlled. One advantage with PWM is that it is possible to control both amplitude and frequency of the inverter output. Another advantage is that the output only has high order harmonics which is easily filtered out, it is, however, more complicated than square wave mode [20].

PWM can be either bipolar or unipolar. In bipolar PWM one sinusoidal control signal is compared with the triangular waveform and the switches work in the pairs  $TA+$ ,  $TB-$  and  $TB+$ ,  $TA-$  such that the output from leg B is the negative of leg A. In unipolar PWM two sinusoidal control signals are compared with the triangular waveform. Thus, the legs are not switched simultaneously. This allows the inverter to double the frequency with less harmonics [20].

Square wave mode is a simplified bipolar PWM where  $TA+$ ,  $TB-$  and  $TB+$ ,  $TA-$  are operated in pairs with a fixed duty cycle of 0.5. A disadvantage of using square wave mode is that only the frequency can be controlled. Therefore the DC source must be adjusted to control amplitude. Another disadvantage is that the output will contain low order harmonics. An advantage however is that the control is less complicated than PWM [20].

Voltage cancellation, or phase shift as it is sometimes called, is based on square wave mode and unipolar PWM. The legs are controlled separately but with a fixed duty cycle of approximately 0.5 resulting in an output voltage being a combination of sinusoidal and square wave. The output waveforms can be seen in Figure 2.14. This allows both magnitude and frequency control. The harmonic content is higher than in PWM but lower than square wave mode. However, the control is still less

complicated compared to PWM [20].

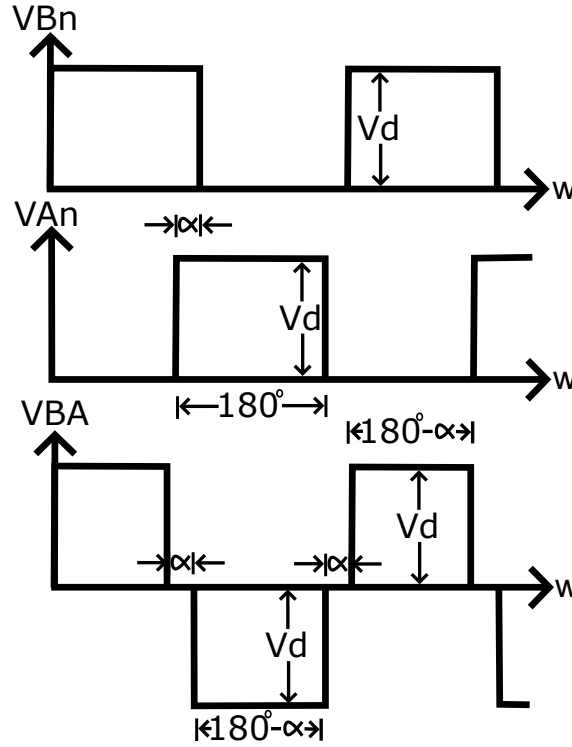


**Figure 2.14:** Theoretical Voltage output from an inverter

In practice the switches take some time to turn on and turn off. If the two switches in one leg are on at the same time it will cause short circuit. Thus, it is necessary to have a short time where both are off. This is called blanking time. This will introduce low order harmonic in the output but is necessary to avoid to short circuit the legs. The output rms voltage can be calculated as

$$V_{out} = V_d * \frac{180 - \alpha}{180} \quad (2.33)$$

where  $V_d$  is the input DC voltage [V] and  $\alpha$  is the time [s] the leg potentials overlap, which can be seen in Figure 2.14 [20].

The losses in the inverter can be divided into switching losses and conduction losses. The switching losses occur when the switches are going from on-state to off-state and vice verse. They occur since the current and voltage through the switch normally change at the same time but not instantaneously. The losses are calculated in the same way for both on- and off-switching as

$$P_{SW} = \frac{1}{T} \int_{t_1}^{t_2} V_{sw}(t) I_{sw}(t) dt \quad (2.34)$$

where  $V_{sw}(t)$  [V] is the voltage across one transistor,  $I_{sw}(t)$  [A] is the current through one transistor,  $t_1$  [s] is the time when the voltage  $V_{sw}(t)$  starts to increase and  $t_2$  [s] is the time when the current  $I_{sw}(t)$  decrease to zero for the off switch state. The



opposite applies for the on switch state. For a full bridge inverter the switching losses is the sum of all switching losses for the four transistors [20].

Since the transistors have internal resistance there are also losses within the transistors, conduction losses, which occur when the switches are leading current. The conduction losses in one switch is calculated as

$$P_{COND} = \frac{1}{T} \int_{t_{on}}^{t_{off}} V_{sw}(t) I_{sw}(t) dt \quad (2.35)$$

where  $t_{off}$  is the time when the voltage begins to rise and  $t_{on}$  is the time when  $V_{sw}(t)$  has reached zero. The total conduction losses for a full bridge converter is four times  $P_{cond}$ . The total losses for a full bridge inverter is therefore given by

$$P_{loss} = 4(P_{COND} + P_{SW}) \quad (2.36)$$

The losses in an inverter turns into heat which also can be used to calculate total losses. This is calculated by

$$P_{heat} = \frac{T_j - T_a}{\theta_{JA}} \quad (2.37)$$

where  $T_j$  is the temperature [°C] measured in the heat sink,  $T_a$  is the room temperature [°C] and  $\theta_{JA}$  (J junction, A ambient) is the thermal resistance [°C/W] in the heat sink [20].



# 3

## Analytical calculations

To be able to analyze the resonant IPT circuit some assumptions must be made, and since it is desirable to be able to compare the calculated values with the values obtained in the experimental tests, some practical limitations must be clarified.

The inverter used in this project is built at the division of Electric Power Engineering at Chalmers University of Technology. Since it is good to have high frequency to achieve high efficiency its' maximum frequency of 200 kHz is used. It is assumed that this is far below self-resonance. Since the frequency used is high, a copper litz wire is used to decrease skin effect.

The loads available in the lab are 10 - 50 W, 12 V halogen lamps. Since lamps are nonlinear (the resistance increase with temperature) the loads used for calculation are 5 and 20  $\Omega$ .

Mutual inductance depends on the size of the coils and the distance between them. By means of Equation 2.30 the graph in Figure 3.1 can be obtained. Parameters  $a$  and  $b$  represents the radius of the sending coil and the receiving coil respectively. The y-axis shows the mutual inductance and the x-axis shows the distance between the coils over radius  $a$ .

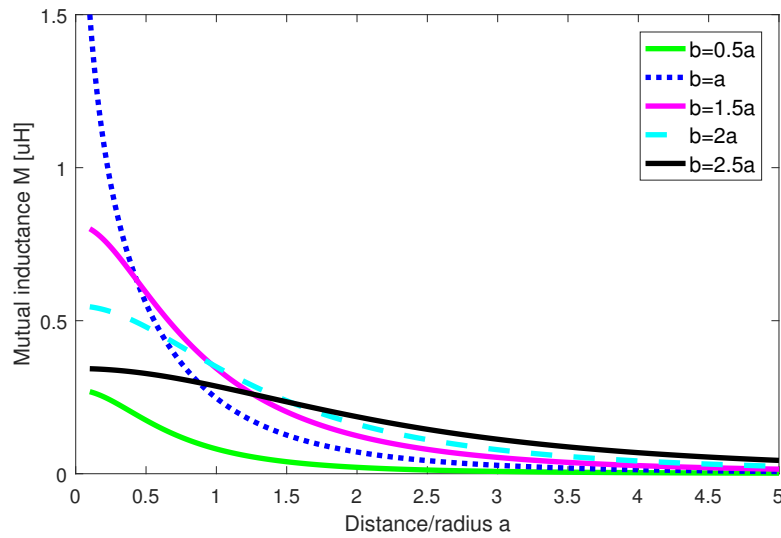


**Figure 3.1:** Graph showing the mutual inductance in terms of the radius of the coils.

### 3.1 Two-coil system

The air gap between the sending coil and receiving coil in this project is set to one meter. The region between near-range and mid-range is when the largest coil diameter and the air gap is equal each other. Hence, the radius of the coils is maximum 0.5 meter. Table 3.1 shows how the mutual inductance vary when either  $a$  or  $b$  is set to maximum radius.

**Table 3.1:** Calculated mutual inductance for single loops in air

Colour	a [m]	b [m]	$M_0$ [ $\mu$ H]
Green	0.5	0.25	0.021
Blue	0.5	0.5	0.071
Magenta	0.33	0.5	0.053
Cyan	0.25	0.5	0.042
Black	0.2	0.5	0.044

It can be seen that highest mutual inductance is reached when both  $a$  and  $b$  equal 0.5 m. By observing Equation 2.9 it can be seen that mutual inductance is proportional to the coupling factor. Thus, if mutual inductance for one turn is increased the coupling factor is increased. When both the coils have a radius of 0.5 m at one meter distance the couplings factor is calculated to 0.0167.

Due to the varying load the SS topology explained in Section 2.3.1 is used in this project. It is assumed that a current of maximum 20 A rms will flow through the wires. Hence, an educated guess is that the wire radius needs to be approximately 8 mm. With this information the self inductance of a single turn of the coils can be calculated to 4.25  $\mu$ H by using Equation 2.29.

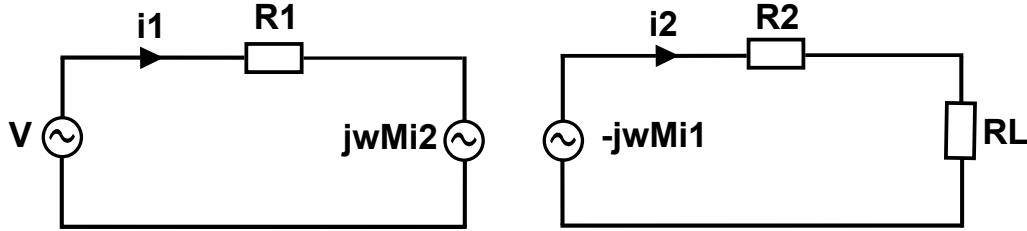
Since the frequency is high, the AC resistance is expected to be significant despite using litz wire. Thus, the AC resistance for a single turn is calculated according to Equation 2.25 to 0.081  $\Omega$  for a single turn.

What remains to be decided is  $N_1$ ,  $N_2$ ,  $C_1$ , and  $C_2$ . Since mutual inductance and the resistance of the coils are dependent on  $N_1$  and  $N_2$ , these are varied to see how current, voltage, and efficiency are affected.  $N_1$  and  $N_2$  decide  $L_1$  and  $L_2$  which in turn sets the values of  $C_1$  and  $C_2$ . All the known values are summarized in Table 3.2.

**Table 3.2:** Calculated and known parameters

Known parameters	Values
$f$	200 kHz
$r_{coil}$	0.5 m
$r_{wire}$	8 mm
$\sigma_{Cu}$	60 MS/m
$V$	12 V
$R_L$	5 and 20 $\Omega$
$M_0$	0.071 $\mu\text{H}$
$L_0$	4.25 $\mu\text{H}$
$R_0$	0.081 $\Omega$

When the inductance is fully compensated the circuit can be redrawn as shown in Figure 3.2.


**Figure 3.2:** Fully compensated circuit with two-coil system

The input current  $i_1$  and the load current  $i_2$  are derived from Section 2.2.1 as

$$i_1 = \frac{V}{R_1 + \frac{\omega^2 M^2}{R_2 + R_L}} \quad (3.1)$$

$$i_2 = -\frac{j\omega MV}{(R_2 + R_L)R_1 + \omega^2 M^2} \quad (3.2)$$

The calculated input current, load current, and efficiency when some values of  $N_1$  and  $N_2$  are varied with a load of 5  $\Omega$  is shown in Table 3.3.

**Table 3.3:**  $N_1$  and  $N_1$  varied to evaluate voltage, current, and efficiency with a 5  $\Omega$  load

$N_1$	$N_2$	$I_1$	$I_2$	$V_L$	Efficiency [%]
1	1	145	2.54	12.72	1.86
1	10	55.07	8.45	42.23	53.97
1	20	21.39	5.76	28.79	64.56
2	1	71.16	2.5	12.48	3.65
2	10	16.92	5.19	25.95	66.33
2	20	5.77	3.1	15.52	69.49

In the same way is  $N_1$  and  $N_2$  varied for a load of 20  $\Omega$ . These values are summarized in Table 3.4.

### 3. Analytical calculations

---

**Table 3.4:**  $N_1$  and  $N_2$  varied to evaluate voltage, current, and efficiency with a  $20\ \Omega$  load

$N_1$	$N_2$	$I_1$	$I_2$	$V_L$	Efficiency [%]
1	1	147.08	0.65	13.06	0.48
1	10	100.53	4.31	86.11	30.73
1	20	52.6	4.34	86.72	59.58
2	1	73.17	0.65	12.99	0.96
2	10	38.09	3.26	65.24	46.57
2	20	16	2.64	52.75	72.53

From the tables it can be seen that the highest efficiency for these number of turns is reached when  $N_1 = 2$  and  $N_2 = 20$ . The obtained circuit parameters with  $N_1 = 2$  and  $N_2 = 20$  are shown in Table 3.5.

**Table 3.5:** Calculated parameters

Calculated parameters	Values
$M$	$2.84\ \mu\text{H}$
$L_1$	$17\ \mu\text{H}$
$L_2$	$1700\ \mu\text{H}$
$R_1$	$0.162\ \Omega$
$R_2$	$1.624\ \Omega$
$\eta_5$	$69.49\ \%$
$\eta_{20}$	$72.53\ \%$

The large inductance of the receiving coil and the high frequency gives a voltage of approximately 6 kV over the coil.  $C_1$  and  $C_2$  can be calculated by Equation 2.18 to 37.25 nF and 372.5 pF respectively.

The Q-factors and bandwidth are calculated for the two loads by using Equations 2.20 and 2.21. The results are summarized in Table 3.6. From the table it can be observed that the  $5\ \Omega$  load's secondary side Q-factor is very high which gives a very narrow bandwidth.

**Table 3.6:** Calculated bandwidth and Q-factors

	$Q_1$	$\Delta f\ 1\ [\text{kHz}]$	$Q_2$	$\Delta f\ 2\ [\text{kHz}]$
<b>5 <math>\Omega</math></b>	8.44	23.7	429.77	0.5
<b>20 <math>\Omega</math></b>	33.74	5.9	107.44	1.9

With a radius of 0.5 m the wire length of each turn is calculated to 3.14 m. With 20 turns on the receiving coil the length of the wire is calculated to 62.83 m and the sending coil wire length is calculated to 6.28 m. With use from Equations 2.22 and 2.18 the stray capacitance of the receiving coil can be calculated to 5.31 pF assuming the speed is 0.7 of speed of light. Since the stray capacitance of

the receiving coil, which is much larger than the sending coil, is small the sending coil stray capacitance is neglected.

## 3.2 Four-coil system

When the inductances are compensated in the four-coil system the circuit can be redrawn as shown in Figure 3.3.

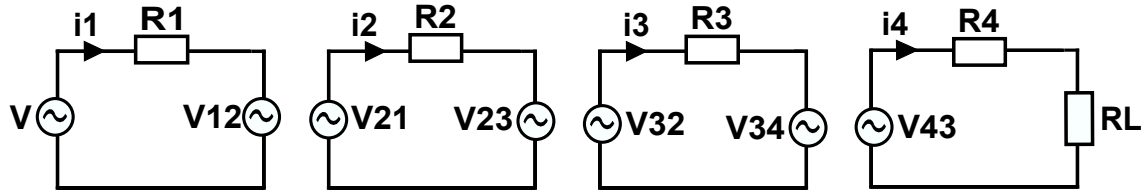


**Figure 3.3:** Fully compensated circuit with four-coil system

By rewriting the equations in Section 2.2.2 to a linear system on the form  $AX=B$ ,  $i_1$ ,  $i_2$ ,  $i_3$  and  $i_4$  can be simply solved using LU factorization with partial pivoting or Gaussian elimination to find the reduced row echelon form.

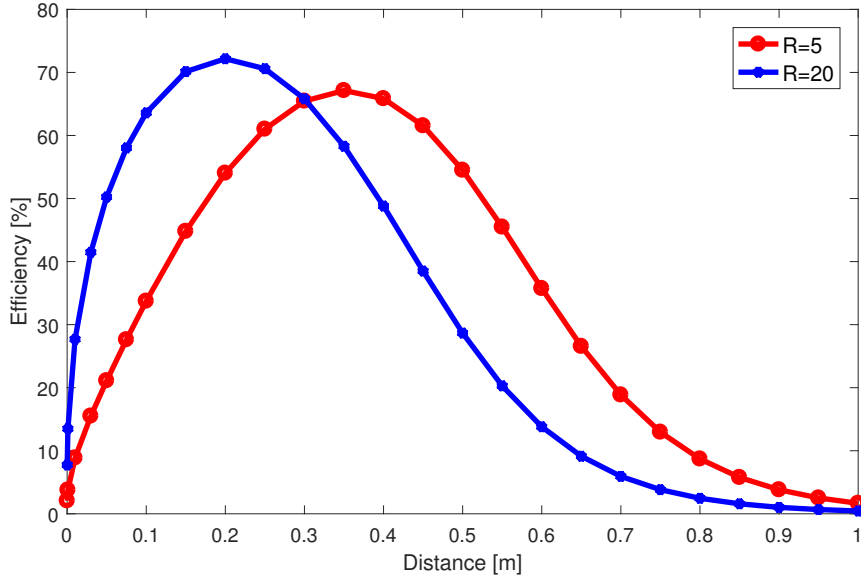
$$\begin{bmatrix} R_1 & j\omega M_{12} & 0 & 0 \\ -j\omega M_{12} & R_2 & -j\omega M_{23} & 0 \\ 0 & j\omega M_{23} & R_3 & -j\omega M_{34} \\ 0 & 0 & -j\omega M_{34} & (R_L + R_4) \end{bmatrix} \begin{bmatrix} i_1 \\ i_2 \\ i_3 \\ i_4 \end{bmatrix} = \begin{bmatrix} V \\ 0 \\ 0 \\ 0 \end{bmatrix}$$

The distance between coil 2 and 3 in the four-coil system is 1 m (the same as for coil 1 and 2 in the two-coil system). Therefore  $M_{23}$  in this system is known. What remains to decide is  $M_{12}$  and  $M_{34}$ . Since the distance between coil 1 and 2 is small, the ratio of distance and radius seen in Figure 3.1 is small. Thus, the mutual inductances,  $M_{12}$  and  $M_{34}$ , are larger if the radius of coil 1 and coil 2 is equal to the radius of coil 3 and 4. To reduce the complexity of the system in the calculations the coil radius is the same for all coils. The source coil and the load coil are single loops, hence the resistance and the self inductance is already known from Section 3.1. The known parameters of the four-coil system is presented in Table 3.7.

**Table 3.7:** Calculated and known parameters of the four-coil system

Known parameters	Values
$f$	200 kHz
$L_1$	4.25 $\mu\text{H}$
$L_2$	17 $\mu\text{H}$
$L_3$	1700 $\mu\text{H}$
$L_4$	4.25 $\mu\text{H}$
$R_1$	0.081 $\Omega$
$R_2$	0.162 $\Omega$
$R_3$	1.624 $\Omega$
$R_4$	0.081 $\Omega$
$M_{23}$	2.84 $\mu\text{H}$

As Section 2.4 explains the advantage of a four-coil system is that the coupling factors  $k_{12}$  and  $k_{34}$  can be adjusted to tune the circuit.  $k_{12}$  and  $k_{34}$  are changed by adjusting the distance between the coils. Thus, the mutual inductance,  $M_{12}$  and  $M_{34}$ , are also affected according Equation 2.11. Figure 3.4 shows how the efficiency of the system with load  $R_L = 5 \Omega$  and  $R_L = 20 \Omega$  vary when the distances  $d_{12}$  and  $d_{34}$  varies.

**Figure 3.4:** Efficiency for the two loads with various distance  $d_{12}$  and  $d_{34}$ 

With 5  $\Omega$  the highest efficiency (67.13 %) is reached when the distances  $d_{12} = d_{34} = 0.35$  m and when the load is 20  $\Omega$  the highest efficiency (72.17 %) is achieved when  $d_{12} = d_{34} = 0.2$  m. From this it can be assumed that with higher loads the efficiency increases if the coils gets closer to each other.



By using LU factorization with partial pivoting and by using the distance that gives the highest efficiency according to Figure 3.4 Table 3.8 can be summarized for the  $5\ \Omega$  load.

**Table 3.8:** RMS current and voltage in primary and receiving circuit with a  $5\ \Omega$  load

$I_1$	$V_1$	$P_{in}$	$I_4$	$V_L$	$P_{out}$	Efficiency
8.98 A	12 V	107.7 W	3.8 A	19.01 V	72.3 W	67.13 %

Similarly, when the load is increased to  $20\ \Omega$  Table 3.9 can be summarized. The tables show the source current, the source voltage, the input power, the load current, the load voltage, the load power and the efficiency of the system.

**Table 3.9:** RMS current and voltage in primary and receiving circuit with a  $20\ \Omega$  load

$I_1$	$V_1$	$P_{in}$	$I_4$	$V_L$	$P_{out}$	Efficiency
3.89 A	12 V	46.66 W	1.3 A	25.95 V	33.67 W	72.17 %

By varying the load for both the two-coil system and the four-coil system Figure 3.5 can be derived. The y-axis show the maximum efficiency of the systems and the x-axis show what load that is used.

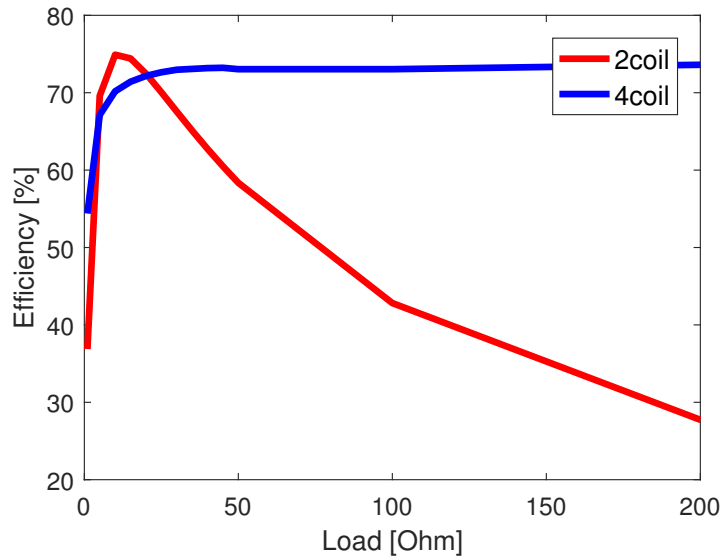


**Figure 3.5:** Efficiency dependent on the load for a two and four-coil system

From the figure it can be observed that the four-coil system is more advantageous to use when the load is increased since it is possible to regulate the system impedance by changing the coupling factors  $k_{12}$  and  $k_{34}$ . It can also be seen that  $5\ \Omega$  and  $20\ \Omega$  appears to be the limit points for which the two and four-coil system have the same efficiency. Between  $5\ \Omega$  and  $20\ \Omega$  the efficiency is higher for a two-coil

### 3. Analytical calculations

---

system. Hence, the two-coil system and the four-coil system is acceptable to use in this project.

# 4

## Electromagnetic field analysis

To verify that the calculated inductances in Chapter 3 are correct and to analyze the magnetic field described in Section 2.1, finite element method (FEM) is used. This is a numerical method to solve differential equations by means of a computer. One program which uses FEM is COMSOL Multiphysics<sup>®</sup>.

Several models were built and investigated in COMSOL. AC/DC module was used, which is used for simulating electric, magnetic, and electromagnetic fields. The models were built in 2D axisymmetric objects, which means that an object's cross section is built in 2D and rotated around an axis. This is done, instead of running the simulations in 3D, to save computational time. The 2D axisymmetric principle is shown, with cross section for a solenoid and a flat coil, in Figure 4.1.

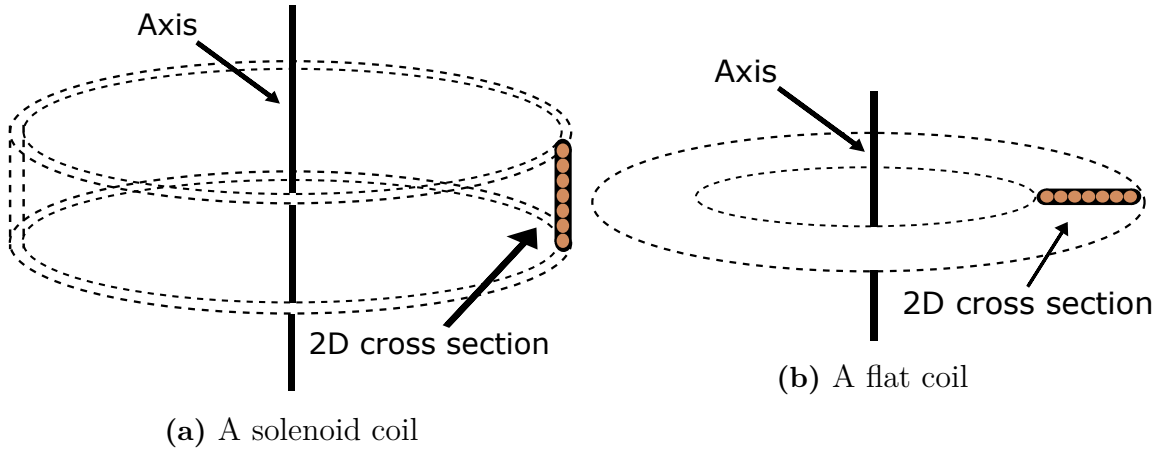


**Figure 4.1:** Two 2D axis symmetric principles

The magnetic fields are studied in frequency domain and the physics used in COMSOL is specified to "Magnetic fields". The boundary conditions for the whole model is given by a ten meter diameter circle with the material air. To build and simulate a simple coil a cross section is built and declared as a homogenized multi-turn coil, which has  $N$  number of turns and is made of copper.

Self inductance is decided by building a coil and excite it with a current. By using Equation 2.7 or 2.8 the self inductance can be calculated. Mutual inductance is decided by building two coils and exciting one of the coils with current. The mutual inductance is calculated by Equation 2.5 or 2.6.

The simulated models are two-coil system using flat coils, two-coil system using solenoid coils, and four-coil system. In the practical setup the wires are separated to decrease the risk of flash overs between the wires. Due to this the simulations was made in two iterations. The first one with the wire wound tightly together, similar to the calculated. The second iteration was performed with some turn ratio, meaning the coils were wound with some air between each turn.

## 4.1 Flat coils

The primary coil has two turns and the secondary coil has 20 turns as decided in Section 2.1. The width of the primary coil is 2 cm and the width of the receiving coil is 12 cm when wounded with some turn ratio. Table 4.1 shows the values of the inductances from the simulation together with the calculated values from Section 3.1. The simulated resistance for the coil with two turns is 0.05622 and the simulated resistance for the coil with 20 turns is 0.56. This is quite low compared to the calculated resistances. This is due to that COMSOL only takes DC resistance into account. By using Equation 2.9 a couplings factor of 0.028 could be calculated by using flat coils.

**Table 4.1:** Simulated inductances using flat coils in Comsol

	$L_1$ [ $\mu\text{H}$ ]	$L_2$ [ $\mu\text{H}$ ]	$M$ [ $\mu\text{H}$ ]
Calculated	17	1700	2.84
Simulated	15.92	1121.76	2.44
Simulated with turn ratio	11.68	862.26	2.83

The inductances calculated with elliptical integrals differs quite a bit from the simulated ones. This could be due to the fact that when calculating the inductances it is assumed that all the turns are at the same place. This increases the inductance. It becomes unquestionable clear that when more turns are used and more space between each turn is used the inductances from the calculation and the simulation differ more.

## 4.2 Solenoid coils

The two turns of the sending coil had a height of 3.2 cm and the 20 turns of the receiving coil had a height of 16 cm when turn ratio was used in the solenoid coils. The magnetic flux caused by a ten ampere current in the primary loop is illustrated in Figure 4.2.

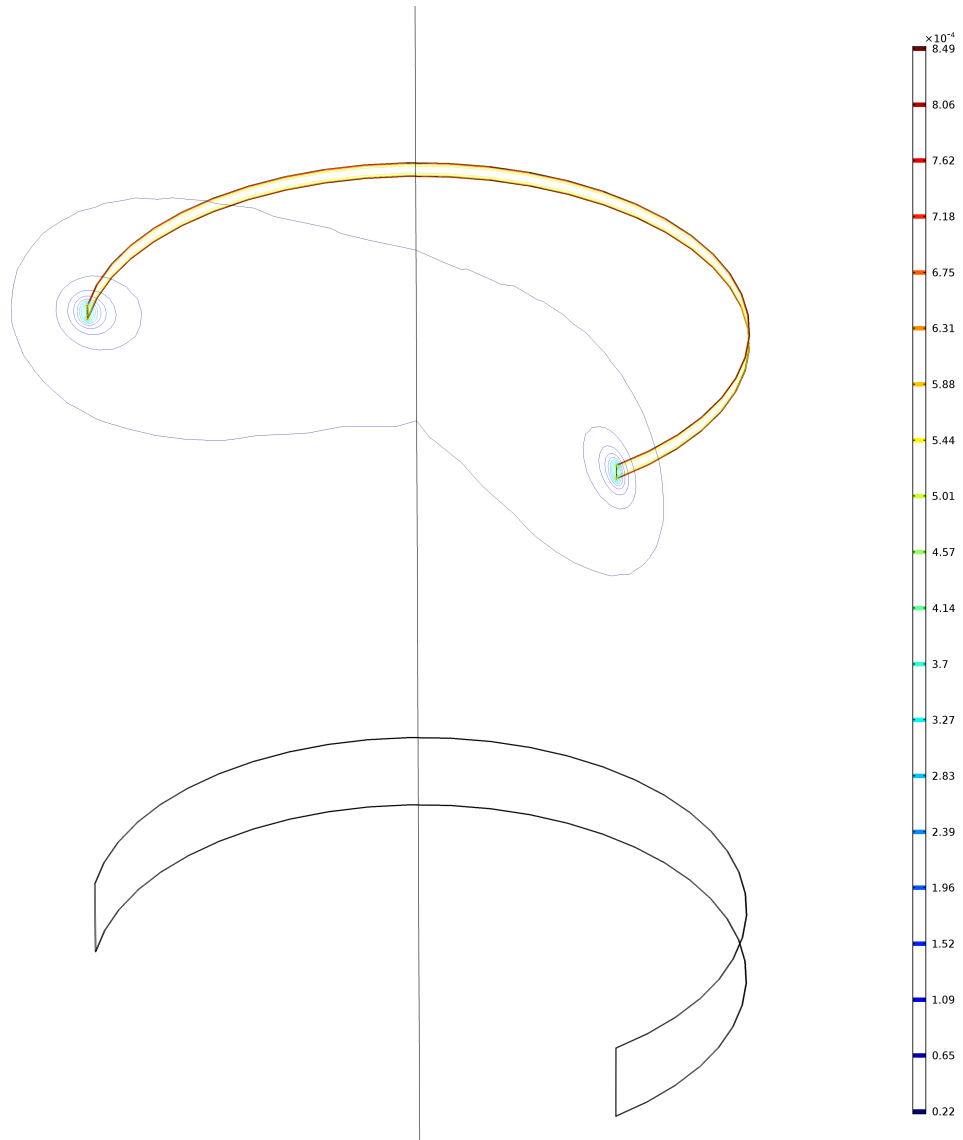


**Figure 4.2:** The magnetic flux density is relatively strong nearby the primary coil at the top and weak in the receiving coil near the bottom

The inductances from the simulation together with the inductances from the calculations are summarized in Table 4.2. The simulated resistance for the coil with two turns is 0.05622 and the simulated resistance for the coil with 20 turns is 0.56. The coupling factor was calculated to 0.026 using Equation 2.9.

**Table 4.2:** Simulated inductances using solenoid coils in COMSOL

	$L_1$ [ $\mu\text{H}$ ]	$L_2$ [ $\mu\text{H}$ ]	$M$ [ $\mu\text{H}$ ]
Calculated	17	1700	2.84
Simulated	15.947	1089.562	2.745
Simulated with turn ratio	11.433	749.693	2.4431

The inductances calculated with elliptical integrals differs quite a bit from the simulated ones here, similarly to the flat coil system. The coupling factor when using

flat coils is somewhat larger compared to using solenoid coil but since using solenoid coils is the least complex model to implement in practice the Q-factors for this coil design are investigated. Furthermore, is magnetic ferrite integrated into the model and analyzed. With the same reasoning the four-coil system is only simulated using solenoid coils.

### 4.2.1 Q-factors

The simulated Q-factors for the two loads are calculated by using Equation 2.20 and Equation 2.21. The results are summarized together with the analytically calculated Q-factors in Table 4.3. It can be observed that the Q-factors are lower than the calculated values, which makes the systems less difficult to tune.

**Table 4.3:** Calculated and simulated bandwidth and Q-factor

	$Q_1$	$\Delta f$ 1 [kHz]	$Q_2$	$\Delta f$ 2 [kHz]
<b>5 <math>\Omega</math></b>				
calc	8.44	23.7	429.77	0.5
sim	7.62	26.3	188.42	1.1
<b>20 <math>\Omega</math></b>				
calc	33.74	5.9	107.44	1.9
sim	30.49	6.6	47.10	4.2

### 4.2.2 Ferrite implementation

Ferrite core is a common way to increase the coupling factor, as mentioned in Section 2.1. Ferrite with an electrical conductivity of  $0.5[S/m]$  and permeability of 2000 were implemented in different constellations in the two-coil system. The results are listed in Table 4.4.

**Table 4.4:** Couplings factor with different use of ferrite ( $\sigma = 0.5[S/m]$  and  $\mu = 2000$ )

Variant	Coupling factor
Without ferrite	0.026
With a ferrite plate at each coil	0.029
With a ferrite core in each coil	0.029
With a common ferrite core	0.411

The highest possible coupling factor is achieved when the two coils have a common very large ferrite core, similar to a regular transformer. The second best option would be to have a ferrite plate at the end of each coil or a ferrite core in the coils to direct the magnetic field. The coupling factor does however not increase enough for it to be worth the extra cost.

### 4.2.3 Electromagnetic fields

High magnetic flux density, alternating magnetic field and electrical field strength could be dangerous to humans. Due to this simulations are performed in COMSOL. Measurements of the fields were collected in six points between and around the coils in coordinates  $(1,0)$ ,  $(1,1)$ ,  $(0,0)$ ,  $(0,1)$ ,  $(0,-1)$ ,  $(1,-1)$ . This is visualized by the blue dots and circles in Figure 4.3

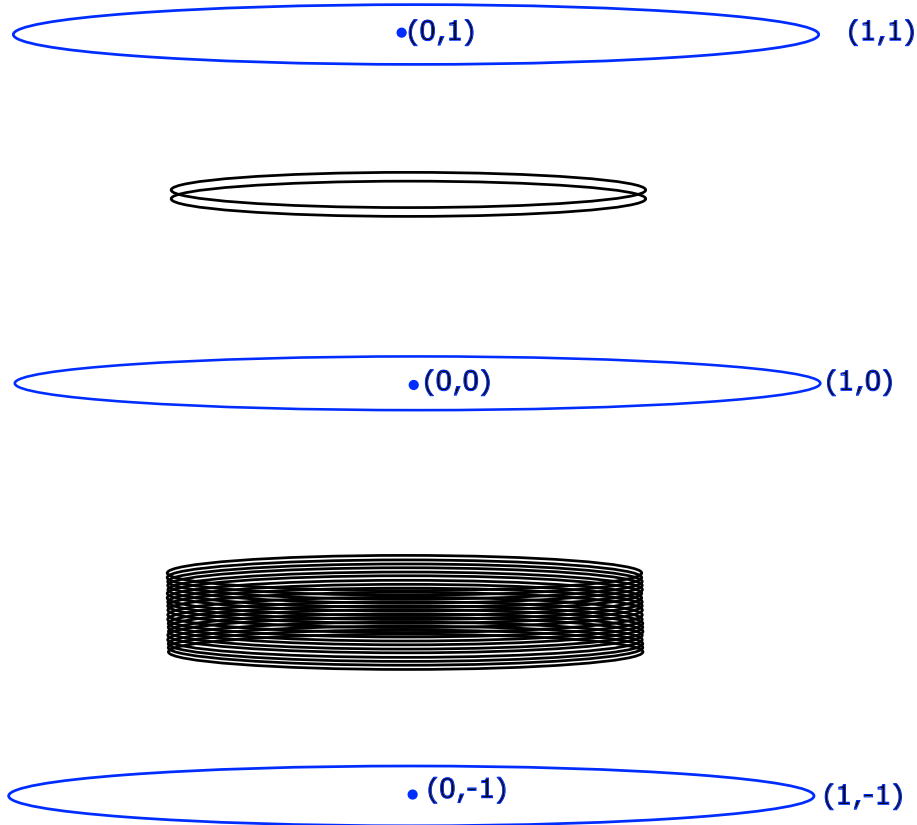
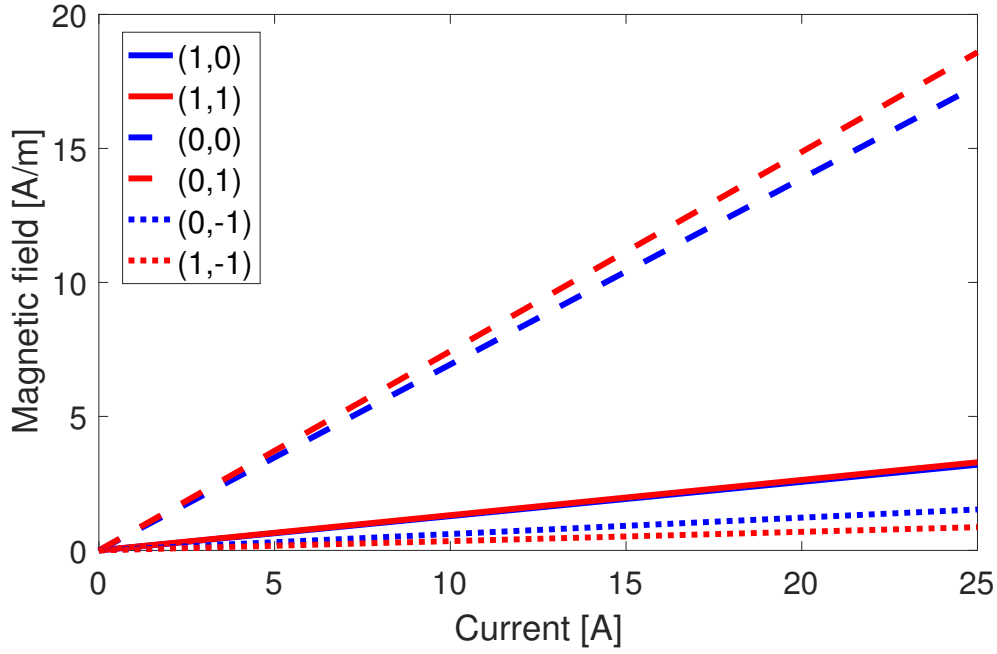
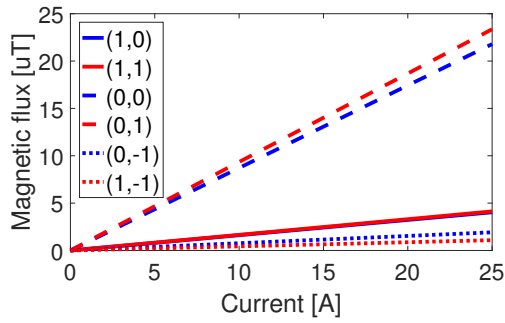


**Figure 4.3:** Points where measurements of magnetic field and flux density as well as electric field were performed

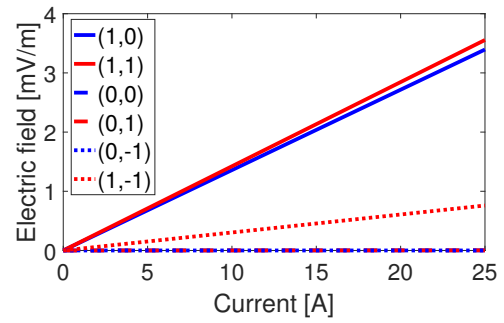
The magnetic field is proportional to the enclosed current in any circuit, as Equation 2.1 shows. Due to this the magnetic field was plotted against the current in the sending coil as can be seen in Figure 4.4a. The magnetic field increases linear with increasing current. Since the magnetic flux is proportional to the magnetic field the flux density will increase accordingly to the magnetic field. Thus with an increasing current an increase in magnetic flux will occur, which is visualized in Figure 4.4b. The last field that could be dangerous for humans is the electric field. Figure 4.4c shows the electrical field as a function of the current in the sending coil.



(a) Magnetic field nearby the coils



(b) Magnetic flux nearby the coils



(c) Electric field nearby the coils

**Figure 4.4:** Magnetic field and flux and electric field nearby the coils

The electrical field is strongest on the outside of both the coils whilst the magnetic field is strongest between the coils.

### 4.3 Four-coil system

The source coil and the load coil have one single turn coil. The sending coil has two turns and the receiving coil has 20 turns as decided in Section 3.1. The geometry for the four-coil system can be visualized in Figure 4.5.



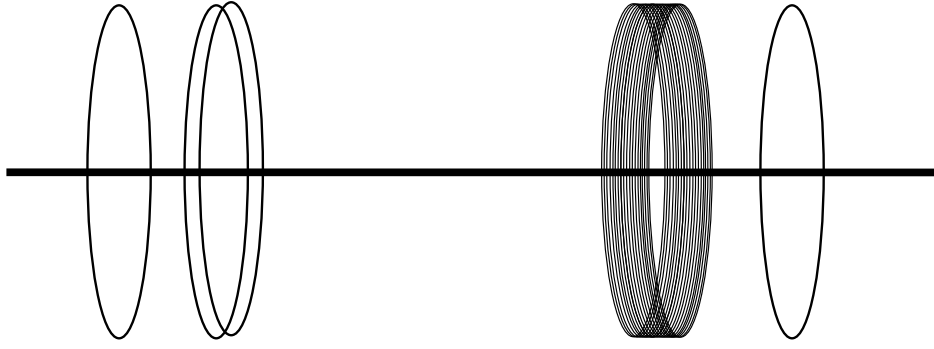


**Figure 4.5:** Principal sketch of a four-coil system simulated in COMSOL

The self inductance of the four coils are simulated as before, one by one, both with and without turn ratio. As expected the self inductance of the sending and receiving coil is as big as in the simulations with just two coils. These values are summarized in Table 4.5. With turn ratio the coupling factors are calculated to:  $k_{12}=0.1082$ ,  $k_{23}=0.0264$ , and  $k_{34}=0.1151$ .

**Table 4.5:** Simulated inductances for the four-coil system

	$L_1$ [ $\mu\text{H}$ ]	$L_2$ [ $\mu\text{H}$ ]	$L_3$ [ $\mu\text{H}$ ]	$L_4$ [ $\mu\text{H}$ ]
Calculated	4.27	17	1700	4.27
Simulated	4.257	15.947	1089.562	4.257
Simulated turn ratio	4.257	11.433	749.693	4.257

As Figure 3.4 shows the maximal efficiency of a four-coil is dependent on the distance  $d_{12}$  and  $d_{34}$  which varies with the load. For a  $5\ \Omega$  load the highest efficiency is achieved when  $d_{12}=d_{34}=0.35\text{ m}$ . Thus the mutual inductance was simulated with this distance and summarized with the calculated mutual inductance for  $5\ \Omega$  in Table 4.6.

**Table 4.6:** Mutual inductance with a  $5\ \Omega$  load and distance  $d_{12}=d_{34}=0.35\text{ m}$

	$M_{12}$ [ $\mu\text{H}$ ]	$M_{23}$ [ $\mu\text{H}$ ]	$M_{34}$ [ $\mu\text{H}$ ]
Calculated	0.785	2.837	7.85
Simulated	0.7814	2.745	7.47227
Simulated turn ratio	0.754589	2.4431	6.500

In a similar way the highest efficiency with a  $20\ \Omega$  load is achieved when  $d_{12}=d_{34}=0.2\text{ m}$  thus the mutual inductance is simulated with this distance and summarized in Table 4.7. With turn ratio the coupling factors are calculated to:  $k_{12}=0.1843$ ,  $k_{23}=0.0264$  and  $k_{34}=0.1909$ .

**Table 4.7:** Mutual inductance with a 20  $\Omega$  load and distance  $d_{12}=d_{34}=0.2$  m

	$M_{12}$ [ $\mu\mathbf{H}$ ]	$M_{23}$ [ $\mu\mathbf{H}$ ]	$M_{34}$ [ $\mu\mathbf{H}$ ]
Calculated	1.3507	2.8372	13.5074
Simulated	1.34165	2.745	12.7068
Simulated turn ratio	1.2858	2.4431	10.7857

# 5

## Electric circuit analysis

The electric circuit models were built and simulated using LTspice. Both two-coil and four-coil system were modelled. The models contain a DC voltage source, an inverter, compensation capacitors, coils, and a load. The simulations were made in two iterations; the first with a load of  $5\ \Omega$  and the second one with a load of  $20\ \Omega$ . The coil's inductance and resistance were picked from COMSOL and the capacitors were assumed to be ideal. The simulations were compared with calculated values for both systems.

The DC voltage source is modelled with an estimated series resistance of  $10\ \text{m}\Omega$ . The inductance of the wires was estimated to  $2\ \mu\text{H}$  and connected in series with the DC voltage source to simulate the inductance of the wires. Since the real inverter has a capacitor of  $20\ \mu\text{F}$  to keep the ripple down it is also simulated in parallel with the DC voltage source. Figure 5.1 shows how the inverter was simulated. The duty cycle was set to 47 % to allow some blanking time to avoid short circuit the inverter, since the transistors are not ideal with rise time and fall time.

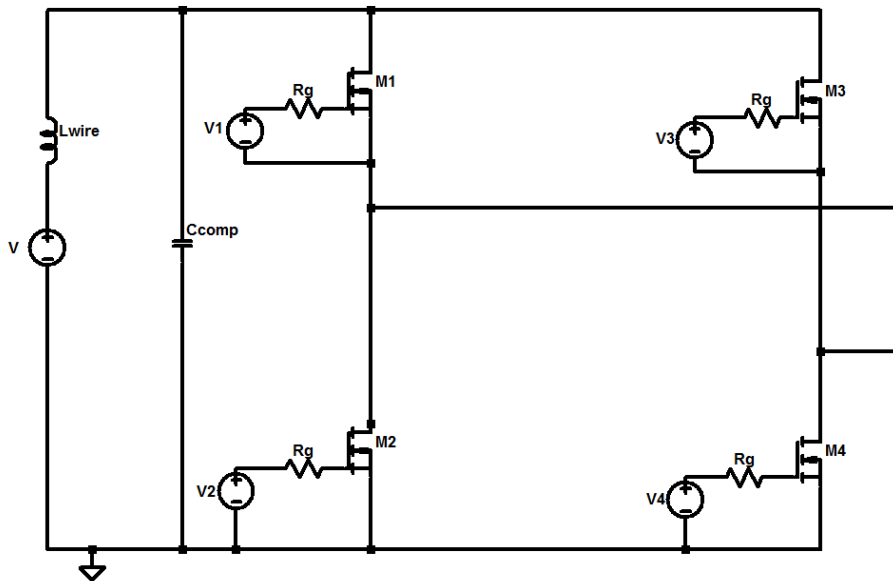


**Figure 5.1:** One-phase full bridge inverter simulated in LTspice

## 5.1 Two-coil system

The two-coil system circuit consists of a primary compensation capacitor, a primary inductance, a secondary compensation capacitor, a secondary inductance and a variable load. The model can be seen in Figure 5.2.

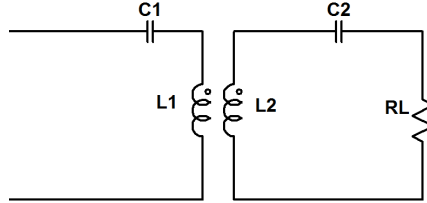


**Figure 5.2:** The resonant circuits of the two-coil system

The coupling factor was set to 0.0264 as the simulations performed in COMSOL indicated. Using Equation 2.18,  $C_1$  is calculated to 55.39 nF and  $C_2$  to 844.69 pF. The voltage and the current in the primary circuit are plotted as well as the current and voltage over the load. Figure 5.3a and 5.3b shows the waveforms with a  $5\ \Omega$  load and Figure 5.3c and 5.3 shows the waveforms with a  $20\ \Omega$  load. In both cases the voltage and current appears to be in phase, which indicates resonance and thus maximizes the transferred power.

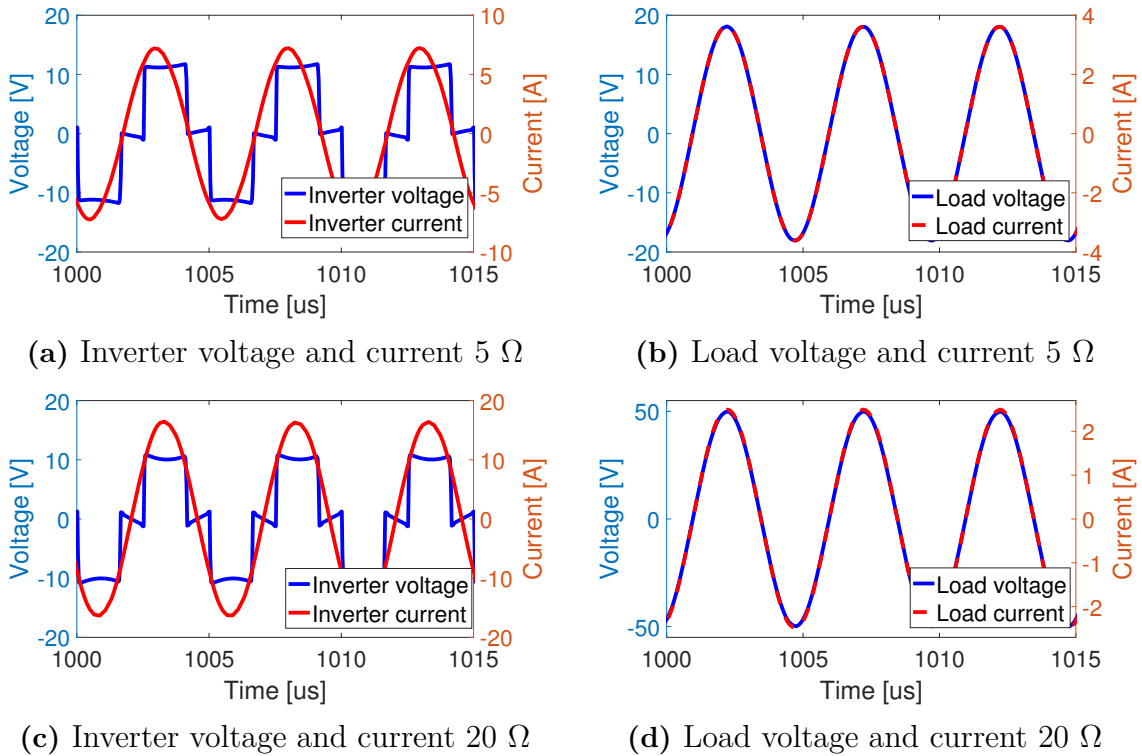


**Figure 5.3:** Simulated waveforms with a two-coil system

To compare the efficiency and the transferred power the rms values from the simulations are compared with the calculated values. In Table 5.1 the simulated values for the  $5\ \Omega$  load with the calculated values are summarized.

**Table 5.1:** Rms current and voltage in primary and receiving circuit with a  $5\ \Omega$  load using two-coil system

	$I_1$ [A]	$V_1$ [V]	$P_{in}$ [W]	$I_2$ [A]	$V_2$ [V]	$P_{out}$ [W]	Efficiency
Calc	5.77	12	69.24	3.1	15.52	48.11	69.6 %
Sim	5.02	9.07	45.53	2.55	12.76	32.54	71.47 %

In a similar way for the  $20\ \Omega$  load the simulated primary current, primary voltage, input power, secondary current, secondary voltage, output power and efficiency are summarized in Table 5.2 together with the same calculated values.

**Table 5.2:** RMS current and voltage in primary and receiving circuit with a  $20\ \Omega$  load using two-coil system

	$I_1$ [A]	$V_1$ [V]	$P_{in}$ [W]	$I_2$ [A]	$V_2$ [V]	$P_{out}$ [W]	Efficiency
Calc	16	12	192	2.64	52.75	139.26	72.53 %
Sim	11.65	8.20	95.53	1.76	35.17	61.9	64.8 %

The efficiency with the  $5\ \Omega$  load are quite similar but efficiency at  $20\ \Omega$  differs approximately 8 %. One of the reasons for this could be since the resistance of the simulated wires are picked from COMSOL and differs a bit from the calculated resistance values.

## 5.2 Four-coil system

The four-coil system was simulated in a similar way to the two-coil system except with four pairs of capacitors and inductances. The four resonant circuits can be seen in Figure 5.4.

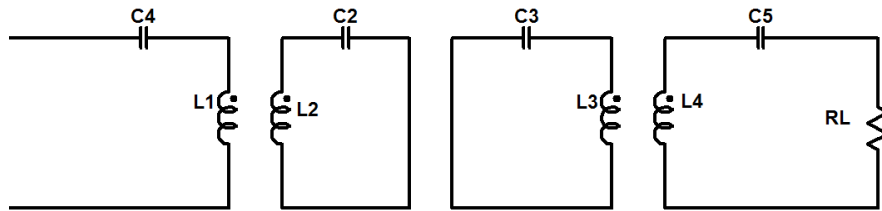


**Figure 5.4:** One-phase inverter together with the resonant circuits of the four-coil system

The resonance capacitors  $C_2$  and  $C_3$  are the same as in the two-coil system (55.39 nF and 844.69 pF.) whilst Equation 2.18 is used to calculate  $C_1$  and  $C_4=14.88\ \mu\text{F}$ .

The three coupling factors for the  $5\ \Omega$  was  $k_{12}=0.1082$ ,  $k_{23}=0.0264$ , and  $k_{34}=0.1151$ , as specified in Section 4.3. For  $20\ \Omega$  they were  $k_{12}=0.1843$ ,  $k_{23}=0.0264$ , and  $k_{34}=0.1909$ . The voltage and current in the sending and receiving circuit are plotted for  $5\ \Omega$  in Figure 5.5a and 5.5b and for  $20\ \Omega$  in Figure 5.5c and 5.5d.

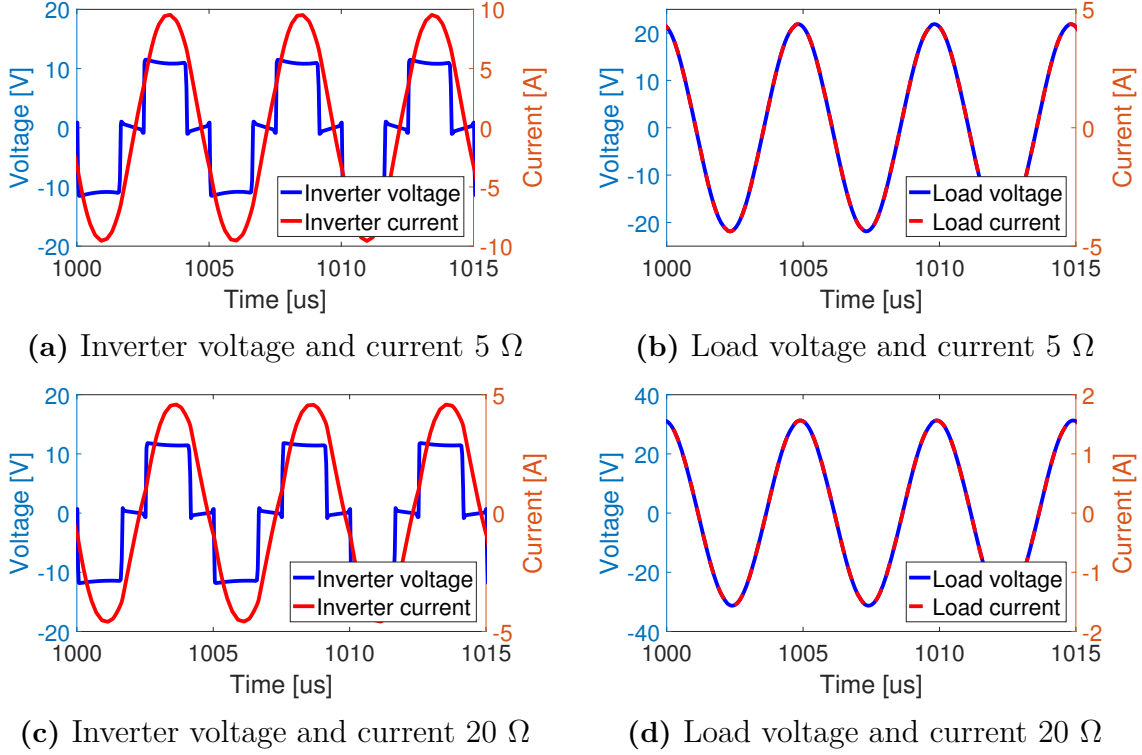


**Figure 5.5:** Simulated waveforms with a four-coil system

Since the current and voltage appears to be in phase in both circuits and at both loads the circuits can be seen as purely resistive and the efficiency should be maximized. Table 5.3 summarizes the simulated and calculated values for the  $5\ \Omega$  load.

**Table 5.3:** RMS current and voltage in primary and receiving circuit with a  $5\ \Omega$  load using four-coil system

	$I_1$ [A]	$V_1$ [V]	$P_{in}$ [W]	$I_2$ [A]	$V_2$ [V]	$P_{out}$ [W]	Efficiency
Calc	8.98	12	107.7	3.8	19.01	72.3	67.13 %
Sim	6.87	8.88	61.02	3.06	15.32	46.96	77 %

In a similar way for the  $20\ \Omega$  load the simulated primary current, primary voltage, input power, secondary current, secondary voltage, output power and efficiency are summarized in Table 5.3 together with the same calculated values.

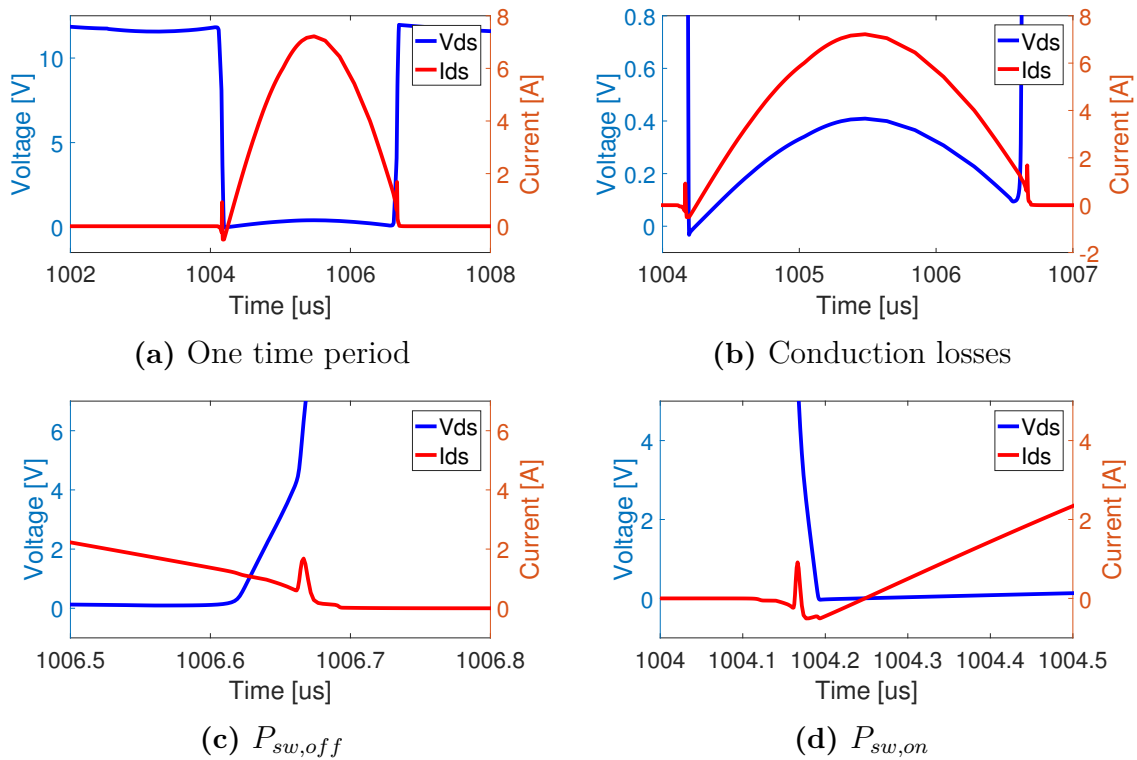
**Table 5.4:** RMS current and voltage in primary and receiving circuit with a 20  $\Omega$  load using four-coil system

	$I_1$ [A]	$V_1$ [V]	$P_{in}$ [W]	$I_2$ [A]	$V_2$ [V]	$P_{out}$ [W]	Efficiency
Calc	3.89	12	46.66	1.3	25.95	33.67	72.17 %
Sim	3.30	9.24	30.49	1.10	22.04	24.25	79.25 %

As Table 5.3 and 5.4 shows the efficiency for the simulated system is approximately 10 % higher than the calculated efficiency for both loads. This could be due to the difference the calculated and simulated values.

### 5.3 Inverter losses

The conduction losses for one switch can be approximated to 0.4332 W from Figure 5.6b by using Equation 2.35 in Section 2.12.  $P_{sw,off}$  can be approximated to 0.08 W From Figure 5.6c by using Equation 2.34 from the same Section. From Figure 5.6d  $P_{sw,on}$  is estimated to zero. The total losses for the inverter can thus be estimated to 2.05 W.

**Figure 5.6:** Switching waveforms from which the inverter losses are estimated





# 6

## Construction of prototype

Since the two-coil model has least complex design but still has a good efficiency at loads used in the experiments (between 5 and 20  $\Omega$ ) it was the only model that was built and compared to the simulation models.

### 6.1 Coil design

To minimize the AC-resistance litz wire is used in the coils. The simulations showed that the maximum rms current in the circuit was about 12 A, thus a qualified guess is that the total area of the wire needs to be at least 1.5 mm<sup>2</sup> to avoid damaging the wires. The skin depth is calculated to 0.147 mm according to Equation 2.24. By assuming that the skin depth needs to be larger than the wire radius the minimum number of strands is calculated by

$$N = \frac{A_{tot}}{A_{strand}} \quad (6.1)$$

where  $A_{total}$  is the total area of the wire,  $A_{strand}$  is the area obtained if the radius of each strand equal the skin depth, and  $N$  is the minimum number of strands needed to avoid large AC resistance. By this assumption the minimum number of strands in the wire is 22. A conductor that fulfills these requirements, with 240 strands, each having a diameter of 0.1 mm, from Electrisola was available in the lab. The total area of this litz is 1.88 mm<sup>2</sup>, hence the assumed wire radius of 0.8 mm which was used in the calculation is still acceptable.

The physical design consist of two solenoid shaped coils. The coils are wired around a wooden frame that is glued together to avoid discharges in screws or nails. Since the simulations and calculations indicated a relatively high voltage over the coils all the turns were separated with a few millimeters to avoid flash-overs. The setup is shown in Figure 6.1.

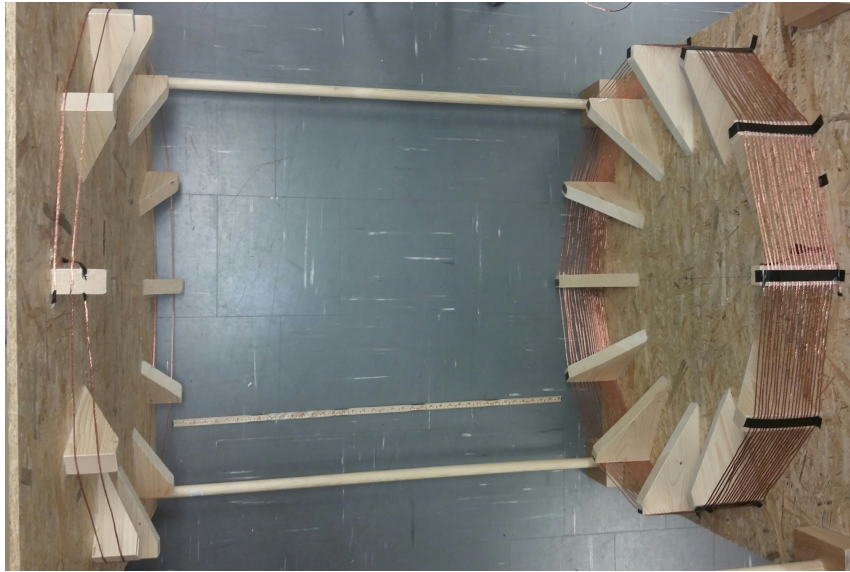


**Figure 6.1:** Sending and receiving coil seen from above

The self inductances were measured with a LCR meter (PEAK electronic design ltd atlas LCR model LCR40). The primary coil with two turns had an inductance of  $13.4 \mu\text{H}$  and the receiving coil with 20 turns had an inductance of  $743.8 \mu\text{H}$ . By measuring the open circuit voltage over the secondary coil and current through the primary coil the mutual inductance was calculated to  $2.63 \mu\text{H}$  by means of Equation 2.6. The inductance values compared with the simulated can be observed in Table 6.1. The variation in values can be due to the physical coil turns are not evenly distributed.

**Table 6.1:** Simulated inductances compared with measured values

	$L_1 [\mu\text{H}]$	$L_2 [\mu\text{H}]$	$M [\mu\text{H}]$	$k$
Simulated values	11.433	749.693	2.4431	0.0264
Measured values	13.4	743.8	2.6322	0.0264

The self resonance frequency of the secondary coil was measured to 722 kHz with the use of a function generator and a booster built by using two BJT transistors. The stray capacitance of the receiving coil could thus be calculated to 65.4 pF using Equation 2.18. This is larger than the calculated stray capacitance for a straight line (5.31 pF), this is however not unexpected since the winding increases the stray capacitance. The primary coil self resonance could not be decided, but since the wire length is much shorter than the secondary coil wire length, it is assumed that the stray capacitance is very small and can thus be neglected.

## 6.2 Compensation capacitors

Since the frequency is high the options regarding capacitors are limited. Electrolyte and super capacitors can not be chosen due to the high frequency (see Table 2.2).

Mica capacitors are expensive and ceramics tends to have higher uncertainty, thus plastic capacitors are used on both primary and secondary side.

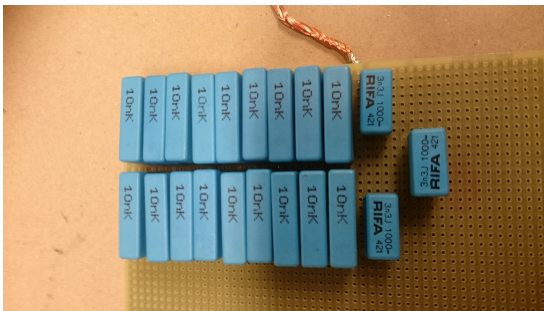
Plastic 3.3 nF, 10 nF and 15 nF capacitors with maximum ratings of approximately 400 V rms and 4 A rms were used in the circuit. According to the LTspice simulations the rms current in the primary circuit is 12 A and the rms voltage over the capacitance is 166 V. The secondary side has a rms current of 1.7 A and the voltage over the capacitance is 1.7 kV. Hence, the current on the primary side and the voltage on the secondary side exceed the maximum ratings of the capacitors.

This can be solved by connecting capacitors in parallel and series to create capacitor banks on the primary and secondary side respectively. At least 3 capacitors in parallel on the primary side and at least 5 capacitors in series on the secondary side is needed not to exceed the maximum rating of one capacitor.

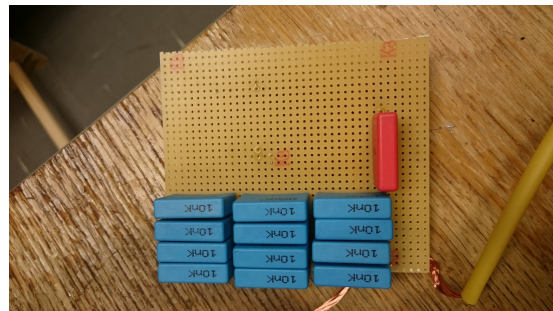
With a frequency of 200 kHz and by taking  $C_{stray}$  into account the capacitance at the secondary side needs to be 47.2 nF and the capacitance at the primary side needs to be 786 pF to achieve resonance.

The primary capacitor bank was built of nine 10 nF capacitors connected in parallel times two in series to get the theoretical capacitance of 45 nF. The measured value was however 46 nF, thus 1 nF was added to the capacitor bank by adding three series connected 3.3 nF capacitors in parallel with the other 18 capacitors, resulting in a measured value of 47.2 nF. This capacitor bank can be seen in Figure 6.2a.

The secondary capacitor bank contains twelve 10 nF capacitors and one 15 nF capacitor in series giving a theoretical value of 789 pF. The measured value was 798 pF but since the difference only is 11 pF it was assumed to be acceptable. The secondary capacitor bank is shown in Figure 6.2b.



(a) Capacitor on the primary side



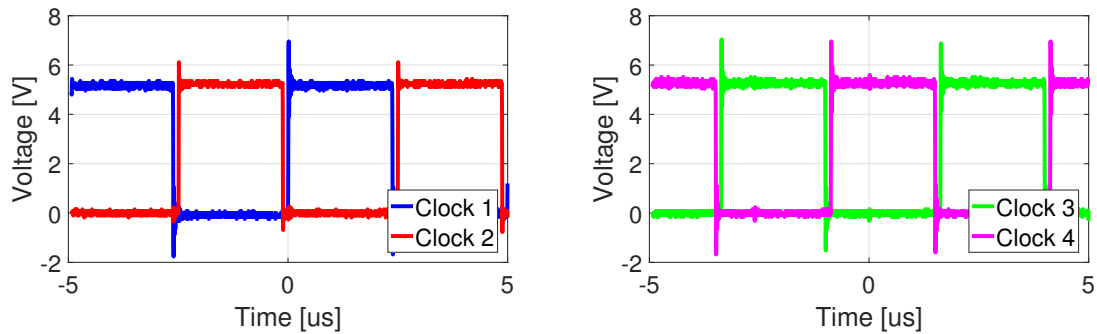
(b) Capacitor on the receiving side

**Figure 6.2:** Capacitors on the primary and secondary side

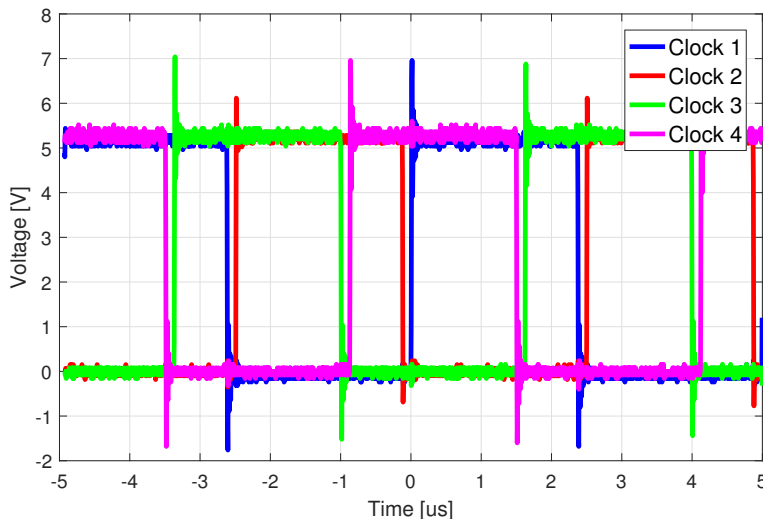
### 6.3 Control of inverter

The microcontroller used to control the inverter is an Arduino Mega. Four clocks of the microcontroller are needed in order to create the control signals for the transistors in the inverter. The chosen frequency of 200 kHz gives a time period of  $5\text{ }\mu\text{s}$  and the duty cycle of all four clocks was programmed to 47 %. The maximum clock frequency of an Arduino limits the steps of the delay and duty-cycle according to  $1/f_{max}$  [21].

The maximum clock frequency of the Arduino Mega is 16 MHz which limits the steps to  $1/16\text{ }\mu\text{s}$ . Hence, the first clock was programmed to start at 0 % of the period time, the second clock was programmed to start at 50 % of the period time, the third was programmed to start approximately 33 % of the period time, and the fourth clock was programmed to start at approximately 83 % of the period time. The measured clock signals can be seen in Figure 6.3.



(a) Waveforms from clock one and two      (b) Waveforms from clock three and four



(c) Waveforms from all the four clocks

**Figure 6.3:** Waveforms from the microcontroller into the inverter

The inverter is, as mentioned in Chapter 3, already available in the lab at the divi-

sion of Electric Power Engineering at Chalmers. It has four SiC power MOSFETs (SCH2080KE) which are controlled with a gate-source voltage from -5 V to 22 V. Since the output voltage of the Arduino is 5 V transistor drivers are needed on all four signals to give a higher voltage to the transistors.

To protect the microcontroller and the power source feeding it from ground currents optocouplers are placed between the microcontroller and the drivers. After the drivers a resistor is connected in series to keep the current down into the transistors. A simple diagram of this circuit can be seen in Figure 6.4.

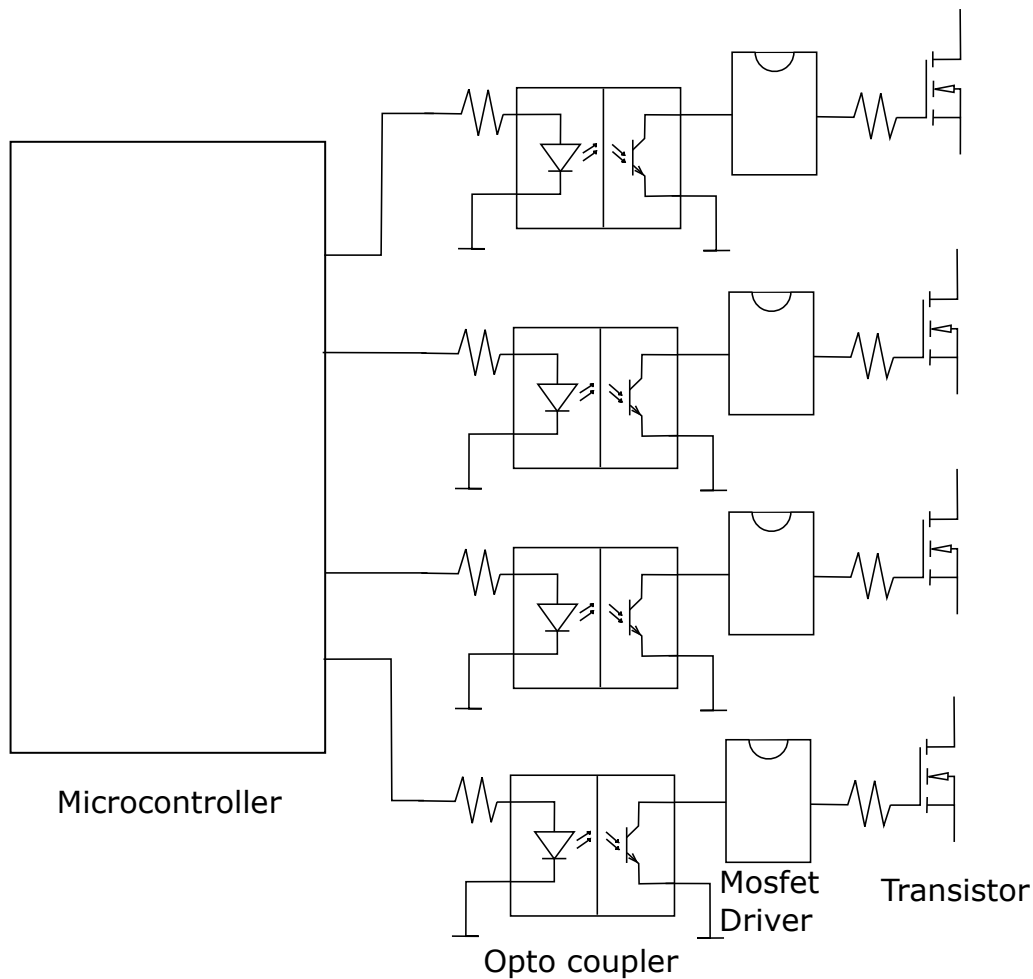


**Figure 6.4:** Simplified graphics of the inverter

## 6.4 Inverter

The inverter is fed with a 12 V DC voltage from a regular DC power supply. The inverter voltage output is shown in Figure 6.5. The voltage waveform out from the inverter looks similar to the simulated voltage. The spikes are due to stray inductances in the transistors.

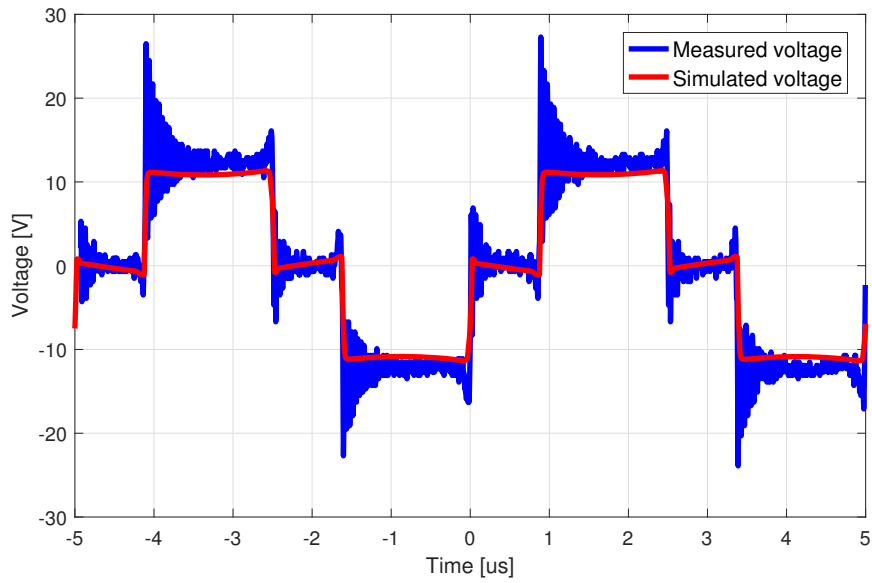
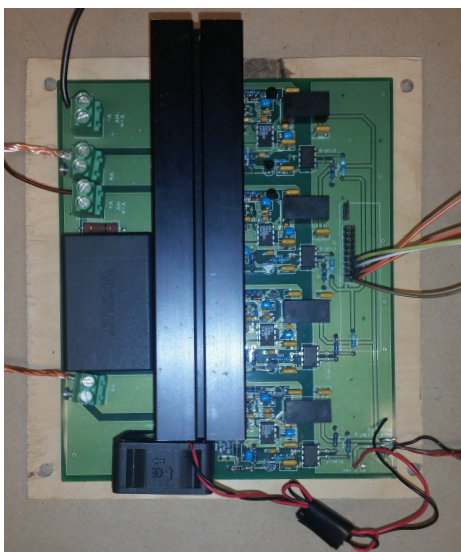
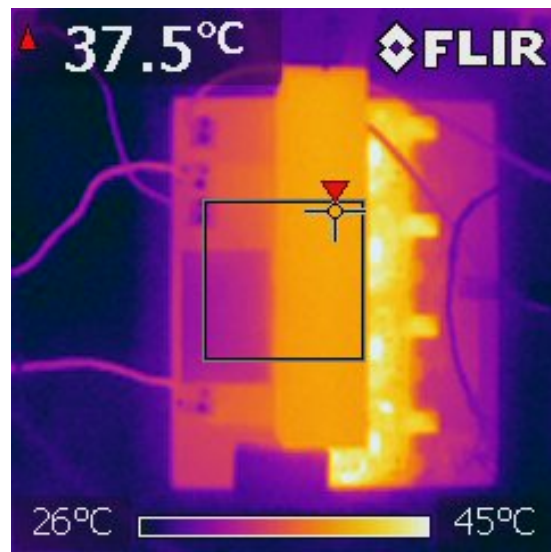


**Figure 6.5:** Voltage out from physical inverter together with simulated voltage

The losses of the inverter were calculated by Equation 2.37 in Section 2.12. The temperature in the heat sinks was after a while measured to 40 °C with a FLIR thermal imaging camera model i7, a measurement of a slightly lower temperature can be seen in Figure 6.6b. The heat sink thermal resistance is estimated to 1 C/W based on similar heat sinks since the used one is unknown. The room temperature is estimated to 25 °C. By this it was estimated that the losses in the inverter is 15 W. This differs from the simulated losses estimated in Section 5.3 which could be due to the oscillation behaviour in the real inverter.



(a) Inverter system



(b) Heat dissipation in inverter

**Figure 6.6:** View of the inverter using normal and heat camera



## 6.5 Q-factor

The simulated and the measured Q-factors can be seen in Table 6.2.

**Table 6.2:** Simulated and measured bandwidth and Q-factor

		$Q_1$	$\Delta f$ 1 [kHz]	$Q_2$	$\Delta f$ 2 [kHz]
5 $\Omega$	sim	7.62	26.3	188.42	1.1
	meas	7.70	26.0	186.94	1.1
20 $\Omega$	sim	30.49	6.6	47.10	4.2
	meas	30.79	6.5	46.73	4.3

The measured Q-factors are similar to the simulated. Thus giving the smallest bandwidth (1.1 kHz) for 5  $\Omega$ .

## 6.6 Test of resonant ITP system

The entire test setup can be seen in Figure 6.7, from right to left, microcontroller, inverter, primary coil and capacitor bank, the air gap and the receiving coil and capacitor bank. The load during this measurement consists of a lamp.

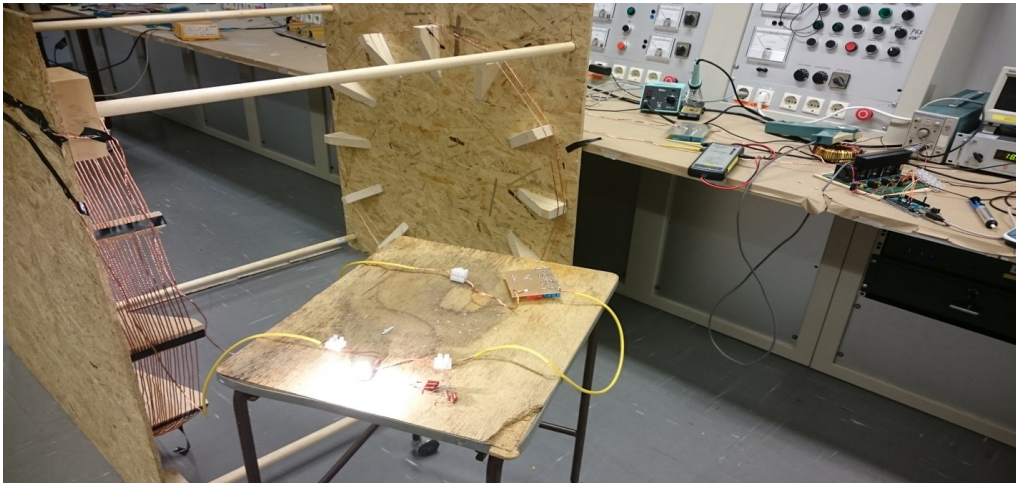


**Figure 6.7:** The entire test setup as it looked in the lab

When the coil wires were moved the resonance was effected. This made the measurements difficult since the the wires moved a little when the measurements were performed. This became particularly clear on the primary side, since the inductance is small. Additionally, the voltage probe used for measurements has a small capacitance, thus affecting the measurements. This became particularly clear on the secondary side, since the capacitance value is low.

Due to the observations on the primary side the input power,  $P_{in}$ , was decided by measuring the DC voltage and current out from the DC power supply and subtracting the power losses from the inverter. This method was assumed to be more accurate than measuring the voltage out from the inverter since the voltage probe affected the resonance.

To ensure that the measurements were accurate the output power,  $P_{out}$ , on the secondary side were conducted by four methods. The first method measures the current and the voltage, the second method measures current and the load resistance, the third method measures voltage and the load resistance, and the fourth method uses a light bulb as load and compares the light it emit to a similar emitting light bulb with known input power. The four methods are summarized in Table 6.3

**Table 6.3:** The four methods to measure the power on the secondary side

Method name	Method	Power
CV	Measure current and voltage	$IV$
CR	Measure current and resistance	$I^2R$
VR	Measure voltage and resistance	$V^2/R$
LC	Comparing emitted lights	$I_{known}V_{known}$

The voltage and current when using the CV method can be seen in Figure 6.8 together with the voltage and the current from the simulated model. The simulated model has been changed to have the real values of inductance and capacitance that were measured. It can be observed from the figure that the voltage and the current appears to be in phase, thus it can be assumed that the secondary side has resonance during this measurement. Furthermore, it can be seen in the figure that the simulated current and voltage waveform have higher amplitude than the measured ones. This could be because there is, despite the litz wire, AC resistance in the wires. This would make the total resistance in the wires in the circuit larger, thus also a larger voltage drop and more losses.

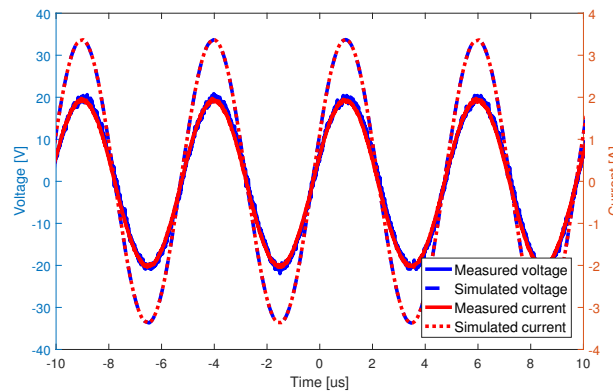


**Figure 6.8:** Comparison between simulated and measured voltage and current over the load



The measured values of three loads are summarized and compared with the simulated values for those loads in Table 6.4.

**Table 6.4:** RMS values of current through the load and voltage over the load

Load ( $\Omega$ )	$i_{2sim}$ (A)	$v_{loadsim}$ (A)	$i_{2meas}$ (A)	$v_{loadmeas}$ (V)
5	2.89	14.5	1.79	9.55
10	2.40	24.0	1.41	14.7
20	1.72	34.4	0.92	19.59

The CV, CR, and VR probe methods used purely resistive loads consisting of Vishay PR03 Series Axial Metal Film Fixed Resistor  $100\ \Omega \pm 5\%$  3 W in different constellations. The measured resistances were 4, 5, 8.4, 10, 14.2, 16.7 and 20  $\Omega$ . The resulting efficiency, together with the simulated ones, can be seen in Figure 6.9.

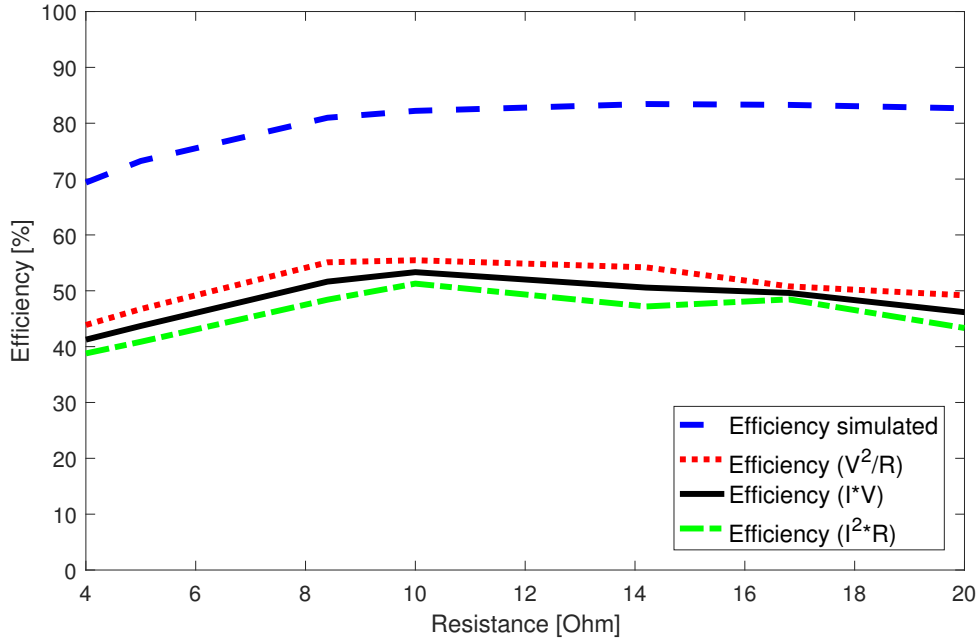


**Figure 6.9:** Graph showing the efficiency of the system with simulations and measurements at different loads

The efficiency of the three methods is clearly lower than the simulated one, which could be a result of a larger voltage drop than anticipated in the wires, as previously mentioned. However, it can be seen in the figure that the three method's result also differs. When the VR method was used the efficiency is approximately 5 % units higher than when the CR method was used. Also the efficiency, when the CV method was used, differs. This shows that the probes affects the measurement and that there are some uncertainties in the measurement equipment.

To verify that the measurements are acceptable, the fourth LC method is used. The LC method's tests were performed using Osram 20 W Capsule Halogen Lamps G4,

12 V, with Stucchi, G4 Base, Halogen Lampholders. Each lamp measured a resistance of  $0.8 \Omega$  cold. The resistance increased with higher temperature. At 20 W the resistance was approximately  $7 \Omega$ .

The first lamp was directly fed from a DC power unit and the second lamp was fed from the resonant IPT system. Since the eye is sensitive to changes in light a comparison could be made by adjusting the DC power unit until the lamps shone with the same strength.

The efficiency of the power transfer was 48 % when  $P_{in} = V \cdot I = 12 \cdot 4.1$  and  $P_{out} = V \cdot I = 13.3 \cdot 1.24$ . The efficiency for each method, with a load of  $7 \Omega$ , is shown in Table 6.5.

**Table 6.5:** Efficiency comparison with  $7 \Omega$

Method	Efficiency [%]
Simulated	74
$V^2/R$	51
$IV$	48
$I^2R$	45
Lamps	48

By this measurement it is decided that the three probe measurements are acceptable but with some uncertainty. To compensate for the AC losses in the simulated model Equation 2.25 is used to calculate the AC resistance to almost three times as big as the DC-resistance, thus giving  $R_1 = 0.168 \Omega$  and  $R_2 = 1.68 \Omega$ . By this assumption the load current and voltage over a  $10 \Omega$  load can be plotted as in Figure 6.10.

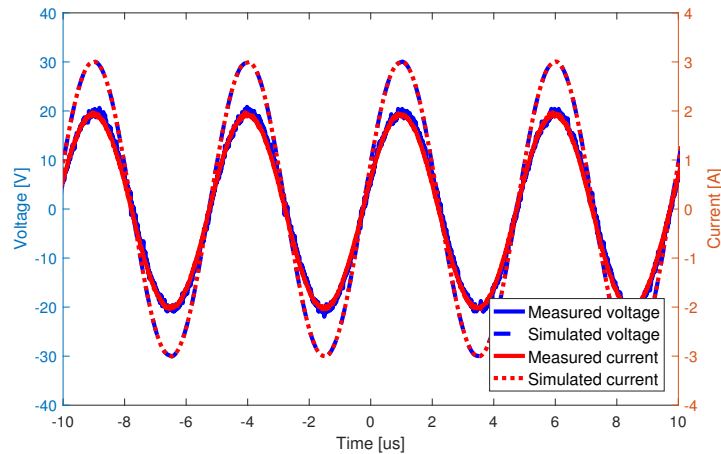


**Figure 6.10:** Comparison between simulated and measured voltage and current over the load with AC-resistance in the coils

When comparing the simulated voltage and current in Figure 6.8 and Figure 6.8 it can be seen that the voltage over the load decreases with approximately 3 V and

the current decreases with approximately 0.5 A when the graphs are plotted with the AC-resistance in the litz wires. The efficiency using AC resistance is plotted in Figure 6.11.

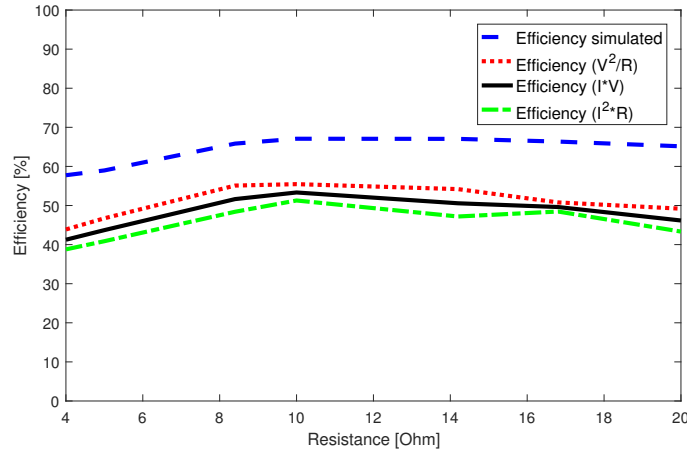
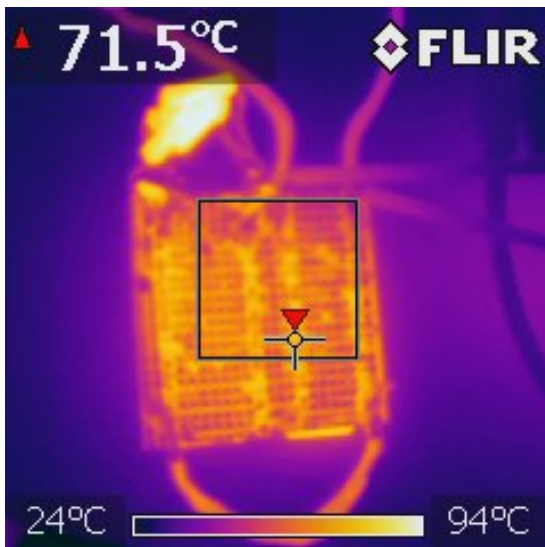


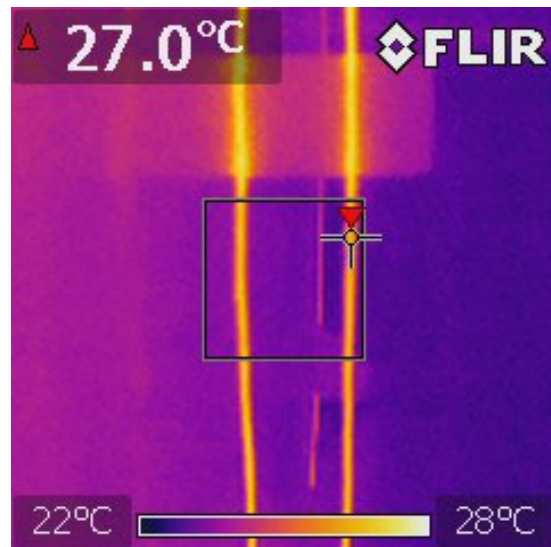
**Figure 6.11:** Efficiency graph with the resistance of the coils simulated with AC resistance

With a higher resistance in the simulated coils the simulated efficiency decreased. At 10  $\Omega$  the simulation is 12-16 % off from the measured values. This could mean that the resonance is not perfect since it is so fragile due to the narrow bandwidth.

It could also be due to discharges in the surroundings, or the generation of heat in the solderings as can be seen in Figure 6.12a and the slight temperature increase in the wire, see Figure 6.12b.



(a) Heat dissipation in the primary capacitor bank



(b) Heat dissipation in the primary wire

**Figure 6.12:** Heatings measured in the primary circuit

A last comparison would be to compare the simulations with measurements with an increasing power. The power voltage increase was performed i steps of 1.5 V. The simulations was made with AC-resistance in the litz wire and a load of  $14\ \Omega$  (the same as two lamps). The losses in the physical inverter were assumed to increase with 1.5 W with the increase in voltage. Table 6.6 was assembled in order to make it comprehensible.

**Table 6.6:** Efficiency measurements with increasing power input

$V_{in}$ [V]	Efficiency sim [%]	Efficiency meas [%]
12	66.99	48.2
13.5	67.04	45.97
15	67.19	44.52
16.5	67.17	42.58
18	67.27	41.03
19.5	67.13	41.67

In the simulations the efficiency was stable around 67 %, the measured efficiency does however decrease with higher input power. This could be due higher discharges in the surroundings or a wrong estimation of heat increase in the inverter.

# 7

## Environmental and ethical aspects

### 7.1 Health aspects regarding exposure to electromagnetic fields

Several studies regarding health aspects of exposure to electric and magnetic fields (EMF emission) have been performed for many years [7]. IARC (International Agency for Research on Cancer) classifies the risk of cancer into four levels [7, 22]:

1. Substances, mixtures and factors that are carcinogenic
2. (a) Substances, mixtures and factors that probably are carcinogenic  
(b) Substances, mixtures and factors that possibly are carcinogenic
3. Substances, mixtures and factors where assessment material is insufficient
4. Substances, mixtures and factors that are probably not carcinogenic

In Sweden, the authority Strålsäkerhetsmyndigheten is responsible for setting the limitations and recommendations for professional as well as general exposure [7]. Table 7.1 shows the recommended values for professional and general exposure regarding electrical fields, magnetic fields and magnetic flux density.

**Table 7.1:** Reference values for fields with frequency ( $f$ ) between 3 kHz and 10 MHz[7]

Type of field	Professional exposure	General exposure
Electrical field strength (E)	0.17 kV/m	0.083 kV/m
Magnetic field (H)	80 A/m	21 A/m
Magnetic flux density (B)	100 $\mu$ T	27 $\mu$ T

Low frequency magnetic fields as well as high frequency electrical fields belongs to group 2b, possibly carcinogenic to humans and static magnetic field is classified to group 3. However, more research regarding what happens to the human body in the intermediate frequency range is needed [7].

### 7.2 Environmental aspects

Copper, which is the main material used in the coils as well as in most electrical components, is a material that exists natural in the earth crust, in rivers, lakes and in the sea [23]. It is an abundant material and the concentration of copper in the

earth crust amounts to 0.000067 %. In the mining areas the concentration of copper is even higher, closer to 0.2-6 % [23]. The demand for copper increases, however, studies show that more copper is recycled. Today approximately 45 % of the used copper comes from recycled material. If the recycling keeps increasing the demand of copper and the environmental impacts will decrease [23].

The copper is extracted from the ground in a mining process. Unregulated mines could be harmful and damaging to the environment and the people working there, in several aspects. Today there are no international laws regulating the mining industry at an international level. The only regulations are national laws, which in some countries companies can avoid by lobbying or bribing [24]. What does exist today is a certificate, ISO 14001, that is used to enforce environmental and mining regulations. Companies have been able to get accredited with ISO 14001 since 1996. The requirements to get the certificate are to participate in education and awareness programs [24].

Wireless charging has become more and more popular in the last decades. In previous master thesis at Chalmers University of Technology near-range wireless power transfer have reached 80-90 % efficiency over a distance of 50 mm [25] and 84.5 % over a distance of 30 mm [26]. In the grey area between near-range and mid-range an efficiency of maximum 77 % has been achieved when distance and coil dimensions are the same [4]. In mid-range applications an efficiency of about 40 % has been accomplished. Hence it can be seen that by increasing the distance between the coils the efficiency of the power transfer decrease. Altogether, by implementing IPT system, compared to having cables in a system, more energy is needed to supply the same amount of energy.

# 8

## Discussion

### 8.1 Areas of opportunity

A wireless every-day could increase the degree of freedom experienced by people. It could theoretically be implemented in almost everything, imagine charging a cell-phone whilst waiting for the bus simply by being nearby the bus stop. Except for the freedom that can be experienced in every-day life, there are also a number of applications where wireless power transfer systems could be implemented to pave the way for other inventions. One example of this could be in the electrification process of vehicles. If IPT systems could be implemented in vehicles and for example at traffic lights the need for bulky and heavy batteries would be decreased and thus the capacity could be increased as well as the weight be decreased.

### 8.2 Future work

The size of the IPT system in this project must be decreased to be practical in many of today's applications. However, normally when considering IPT systems the distance is just a few centimeters. This would also make a downscale of the IPT system possible.

The simulation and the measured values differed. Since the efficiency in the system is affected by the resistance, it can be better to analyze the AC resistance of the whole system more as well as the heat losses due to resistance in the solderings and the capacitors. Furthermore, many assumptions were made, such as losses in inverter which could also be a part in the different values.

The difference in the simulation and in the practical results can also be because by moving the table on which the load and capacitor bank was placed the inductance of the coil was changed. Due to the high Q-factor of the system the resonance was affected a fair amount. This could be solved in the future by having a permanent installation or decreasing the Q-factor in the. Furthermore, the simulations were performed in an ideal world where there are no other objects that could affect the circuit. This should be compared to the laboratory where many things around the coils contain metal.

The voltage probe was problematic when the measurements were performed. When

the voltage probe had physical contact with measurement points a few pF was added to the circuit, which affected the resonance. This was observed in a number of measurements. One example of this was the measurements of the lamp, where it could clearly be seen that when the voltage probe was added the light became brighter.

A high frequency is desired in the IPT system to get good efficiency. The highest frequency that can be used in this system is the self resonance frequency of 722 kHz. It is possible to increase this frequency by changing the design of the coils. However, it is important to consider how much more efficient the power transfer becomes and how much more losses there will be in the inverter, since higher frequency means higher switching losses.

The number of turns of the sending coil was set to two and the number of turns on the receiving coil was set to 20. This made the voltage over the coil and the capacitor on the receiving side very high. Not only can the voltage decrease on the secondary side by having more evenly distributed number of turns on the sending and the receiving side, but the efficiency of the system can be increased for many loads if the number of turns is changed.

### 8.3 Possible health risks

Table 7.1 in Section 7.1 specifies the recommended values for general and professional exposure and in Section 4.2.3 the flux and fields are plotted as a function of the current (see Figure 4.4a, 4.4b, 4.4c). The simulated measurements were performed up to 25 A rms which is a bit higher than what the litz can carry. At 25 A the magnetic field is the only field that is near the recommended limits. The current when the magnetic field hits the maximum recommended field strength of 21 A/m is 28.4 A (since the increase in magnetic field is linear with increasing current). If something similar to this system were used in for example wireless charging zones for phones, the transferred power would also be lower, which would give a lower current and thus a lower magnetic field. However if the systems would be used for higher power applications, for example electric vehicles, the magnetic field would be above the recommended limits.

### 8.4 Environmental aspects

The large coil dimensions together with the many number of turns on the receiving coil made it necessary to use a great deal of copper wire. If this would be implemented, in large scale around the world, it could have a negative affect on the environment if no international laws are established that regulates the copper mines. However compared to a common transformer the amount of copper is not higher.



The simulations showed that the efficiency of the simulation was approximately 70 % and the measurements had an efficiency of approximately 50 %. This low efficiency mean that more energy goes to waste which can have negative impact on the environment if the used electricity is not produced from clean energy sources. However if a IPT system is implemented in roads and electric vehicles, the size of the batteries can be reduced which can be seen as a positive environmental aspect.



# 9

## Conclusion

The two-coil system and the four-coil system was analyzed using elliptic integrals, circuit theory, COMSOL and LTspice. The two-coil system was implemented in reality and a short literature study regarding environmental and ethical aspects was performed.

Analytical calculations using elliptical integrals and circuit theory were performed in order to calculate mutual inductance, number of turns, self inductance, resistance of the coils, coupling factor, voltages, currents, efficiency and compensation capacitors.

Simulations of the coils were performed in 2D axisymmetric using the frequency domain in COMSOL Multiphysics®. This gave the simulated self inductances and mutual inductances for both the two-coil system and the four-coil system. These values were compared to the calculated ones and it was concluded that the values were quite close but that the distance between the turns in the COMSOL model would make the inductances closer to reality.

The results obtained from COMSOL were therefor implemented in a LTspice model. The LTspice model was made up by a DC source, the inverter, the compensation capacitors, the coils and a resistive load. The calculations and the simulations were performed using a  $5\ \Omega$  load and a  $20\ \Omega$  load since the interval between these load values would give a relative high efficiency in the two-coil system.

Using a two-coil system the calculated efficiency was 69.6 % for  $5\ \Omega$  and 72.53 % for the  $20\ \Omega$  load. The simulations gave an efficiency of 71.47 % for the  $5\ \Omega$  load and 64.8 % for the  $20\ \Omega$  load. The four coil system gave a calculated efficiency of 67.13 % for the  $5\ \Omega$  load and 72.17 % for the  $20\ \Omega$  load. The simulated efficiency was 77 % and 79.25 % respectively.

The two-coil system using solenoid coils was implemented in reality and measurements were performed. A microcontroller was programmed to control an inverter with maximum frequency of 200 kHz. The losses in the inverter was calculated to 15 W by measuring the temperature of the heat sinks mounted on the transistors. Since the used inverter could not supply the resonance frequency, capacitor banks made of plastic capacitors were used to compensate for the leakage inductance and copper litz wire was used to avoid too high AC resistance.

The simulated and the measured values differed. Since many values in the system is

affected by the resistance, it can be better to analyze the AC resistance of the whole system further. The difference can also be because by moving the table on which the load and capacitor bank was placed the inductance of the coil changed. Due to the high Q-factor of the system the resonance was affected a fair amount. This could be solved by having a permanent installation in the future. Furthermore, the simulations were performed in an ideal environment while the laboratory where the measurements were performed had many objects containing metal.

The transferred power and the efficiency of the system was measured using a current and voltage probe and subtracting the losses in the inverter. The voltage probe was problematic when the measurements were performed. When the voltage probe had physical contact with measurement points a few pF was added to the circuit, which affected the resonance. Hence, it is assumed that current probe measurement is somewhat more reliable. The current measurements gave an efficiency of 51.27 % and the voltage measurement gave an efficiency of 56.85 %. Thus, the aim to wirelessly transfer power to a resistive load located one meter away with 50 % was achieved.

A literature study was performed in order to investigate how the electric field, magnetic field and magnetic flux might be dangerous to humans. The magnetic field and flux as well as the electric field was simulated in COMSOL, which showed that the flux and fields were within recommended limits even at higher currents than the litz wire could withstand without breaking. The study also contained the environmental aspects regarding material use and efficiency comparison. From this it was concluded that by implementing international laws that regulates copper mines and by integrating the technology into society in a resourceful way the environmental impact can be limited.

# Bibliography

- [1] S. Chopra and P. Bauer, “Analysis and design considerations for a contactless power transfer system,” in *Telecommunications Energy Conference (INT-ELEC), 2011 IEEE 33rd International*, pp. 1–6, IEEE, 2011.
- [2] W. C. Brown, “The history of power transmission by radio waves,” *IEEE Transactions on Microwave Theory and Techniques*, vol. 32, no. 9, pp. 1230–1242, 1984.
- [3] Z. Bi, T. Kan, C. C. Mi, Y. Zhang, Z. Zhao, and G. A. Keoleian, “A review of wireless power transfer for electric vehicles: Prospects to enhance sustainable mobility,” *Applied Energy*, vol. 179, pp. 413–425, 2016.
- [4] S. Y. R. Hui, W. Zhong, and C. K. Lee, “A critical review of recent progress in mid-range wireless power transfer,” *IEEE Transactions on Power Electronics*, vol. 29, no. 9, pp. 4500–4511, 2014.
- [5] A. P. Hu, *Wireless/Contactless Power Supply:-Inductively Coupled Resonant Converter Solutions*. VDM Publishing, 2009.
- [6] B. H. Choi, V. Thai, E. S. Lee, J. H. Kim, and C. T. Rim, “Dipole-coil-based wide-range inductive power transfer systems for wireless sensors,” *IEEE Transactions on Industrial Electronics*, vol. 63, no. 5, pp. 3158–3167, 2016.
- [7] E. Alexandersson, “Induktiv laddning och hälsoeffekter,” *Viktoria Swedish ICT, Göteborg, Västra Götelands Län*, pp. 11–05, 2013.
- [8] D. K. Cheng *et al.*, *Field and wave electromagnetics*. Pearson Education India, 1989.
- [9] Magnetics, “Learn More about Ferrite Cores.” <https://www.mag-inc.com/Products/Ferrite-Cores/Learn-More-about-Ferrite-Cores>. Online; accessed 2017-06-11.
- [10] O. H. Stielau and G. A. Covic, “Design of loosely coupled inductive power transfer systems,” in *Power System Technology, 2000. Proceedings. PowerCon 2000. International Conference on*, vol. 1, pp. 85–90, IEEE, 2000.
- [11] C.-S. Wang, O. H. Stielau, and G. A. Covic, “Design considerations for a contactless electric vehicle battery charger,” *IEEE Transactions on industrial electronics*, vol. 52, no. 5, pp. 1308–1314, 2005.
- [12] S. Cheon, Y.-H. Kim, S.-Y. Kang, M. L. Lee, J.-M. Lee, and T. Zyung, “Circuit-model-based analysis of a wireless energy-transfer system via coupled magnetic resonances,” *IEEE Transactions on Industrial Electronics*, vol. 58, no. 7, pp. 2906–2914, 2011.
- [13] A. Kurs, A. Karalis, R. Moffatt, J. D. Joannopoulos, P. Fisher, and M. Soljačić, “Wireless power transfer via strongly coupled magnetic resonances,” *science*, vol. 317, no. 5834, pp. 83–86, 2007.

- [14] Y. Zhang, Z. Zhao, and K. Chen, “Frequency-splitting analysis of four-coil resonant wireless power transfer,” *IEEE Transactions on Industry Applications*, vol. 50, no. 4, pp. 2436–2445, 2014.
- [15] A. P. Sample, D. T. Meyer, and J. R. Smith, “Analysis, experimental results, and range adaptation of magnetically coupled resonators for wireless power transfer,” *IEEE Transactions on Industrial Electronics*, vol. 58, no. 2, pp. 544–554, 2011.
- [16] C. Nordling and J. Österman, *Physics handbook*. Studentlitteratur, 1987.
- [17] M. Aghaei and S. Kaboli, “On the effect of disorder on stray capacitance of transformer winding in high-voltage power supplies,” *IEEE Transactions on Industrial Electronics*, vol. 64, no. 5, pp. 3608–3618, 2017.
- [18] R. W. P. King *et al.*, *Electromagnetic engineering*. McGraw-Hill book company, inc., 1945.
- [19] ELFA, “Faktasidor,” 2007. Sweden, ELFA AB.
- [20] N. Mohan, T. M. Undeland, and W. P. Robbins, “Power electronics,” *Wiley*, 1988.
- [21] Atmel, “Atmel atmega640/v-1280/v-1281/v-2560/v-2561/v,” 2014. 8-bit Atmel Microcontroller with 16/ 32/64KB In-System Programmable Flash.
- [22] C. J. Portier and M. S. Wolfe, “Assessment of health effects from exposure to power-line frequency electric and magnetic fields,” *NIH publication*, vol. 98, p. 3981, 1998.
- [23] Scandinavian Copper Development Association Sverige, “Kopparkällor.” <http://copperalliance.eu/se/kopparresurser/koppark%C3%A4llor>, 2017. Online; accessed 2017-04-18.
- [24] MIT, Massachusetts Institute of Technology, “Mission 2016: Strategic Mineral Management.” <http://web.mit.edu/12.000/www/m2016/finalwebsite/index.html>. Online; accessed 2017-04-18.
- [25] P. Mattsson and K. Olsson, “High efficiency inductive charging for electric minicars,” *Chalmers University of Technology, Dept. of Energy and Environment*, 2015.
- [26] F. Carlsson and O. Bååth, “Inductive charging for a self-balancing robot,” *Chalmers University of Technology, Dept. of Energy and Environment*, 2016.